

# Optical Fiber Sensors: Working Principle, Applications, and Limitations

Mohamed Elsherif,\* Ahmed E. Salih, Monserrat Gutiérrez Muñoz, Fahad Alam, Bader AlQattan, Dennyson Savariraj Antonysamy, Mohamed Fawzi Zaki, Ali K. Yetisen, Seongjun Park, Timothy D. Wilkinson, and Haider Butt\*

Fiber-optic technology emerged originally for applications in data transmission and telecommunications. However, sensors based on fiber-optics have been developed rapidly because of their excellent sensing performances and capability to function in remote and harsh environments. The usage of fiber-optic sensors has flourished in many fields over the past 30 years due to the fiber-optic's inherent advantages: cost-effectiveness, miniaturized size, light weight, and immunity to electromagnetic interference. This work reviews the fiber-optic sensors based on Bragg gratings, long period gratings, interferometers, surface plasmon resonance, fluorescence, and light diffusion. Brief theory of sensing principle, fabrication method, applications, advantages and disadvantages of the different fiber-optic sensors, are addressed. Recent progress in numerous sensing fields, including environmental, industrial, and biomedical are discussed for each class of fiber-optic sensors. The review highlights the methods and techniques used to overcome the sensing challenges. Finally, prospect of future developments of fiber-optic sensors is summarized.

than that of a human hair (Figure 1a).<sup>[1]</sup> Optical fibers deliver/guide light for long distances with low losses. Single-index optical fibers consist of a transparent core covered with a transparent cladding material of a lower refractive index. The total internal reflection allows for guiding light in the fiber core; however, based on the waveguide analysis the energy of the transferred light is not fully trapped in the fiber core but a portion of the light travels in the cladding as evanescent waves. When the incident light hits the core-clad interface at angles larger than its critical angle, the light is completely reflected and guided in the fiber. In contrast, the incident light which meets the interface at smaller angles is refracted into the cladding to be lost. The critical angle is the minimum angle required to attain the total internal reflection,

which is determined by the refractive index difference between the core and cladding materials.<sup>[2]</sup>

Fibers can be classified into two categories based on the number of guided modes: single-mode and multimode fibers.


## 1. Introduction

An optical fiber is a flexible, transparent, and cylindrical waveguide made of plastic or silica, with diameters slightly thicker

M. Elsherif, M. F. Zaki  
Department of Experimental Nuclear Physics  
Nuclear Research Center  
Egyptian Atomic Energy Authority  
Cairo 13759, Egypt  
E-mail: elsherifmohamed109@gmail.com

A. E. Salih, F. Alam, B. AlQattan, D. S. Antonysamy, H. Butt  
Department of Mechanical Engineering  
Khalifa University of Science and Engineering  
Abu Dhabi 127788, UAE  
E-mail: haider.butt@ku.ac.ae

M. G. Muñoz  
Advanced Materials Research Center  
Technology Innovation Institute  
Abu Dhabi 9639, UAE

 The ORCID identification number(s) for the author(s) of this article can be found under <https://doi.org/10.1002/adpr.202100371>.

© 2022 The Authors. Advanced Photonics Research published by Wiley-VCH GmbH. This is an open access article under the terms of the Creative Commons Attribution License, which permits use, distribution and reproduction in any medium, provided the original work is properly cited.

DOI: 10.1002/adpr.202100371

A. K. Yetisen  
Department of Chemical Engineering  
Imperial College London  
London SW7 2AZ, UK

S. Park  
Department of Bio and Brain Engineering  
Korea Advanced Institute of Science and Technology (KAIST)  
Daejeon 34141, Republic of Korea

S. Park  
KAIST Institute for Health Science and Technology (KIHST)  
Korea Advanced Institute of Science and Technology (KAIST)  
Daejeon 34141, Republic of Korea

T. D. Wilkinson  
Department of Engineering  
University of Cambridge  
Cambridge CB2 1TN, UK

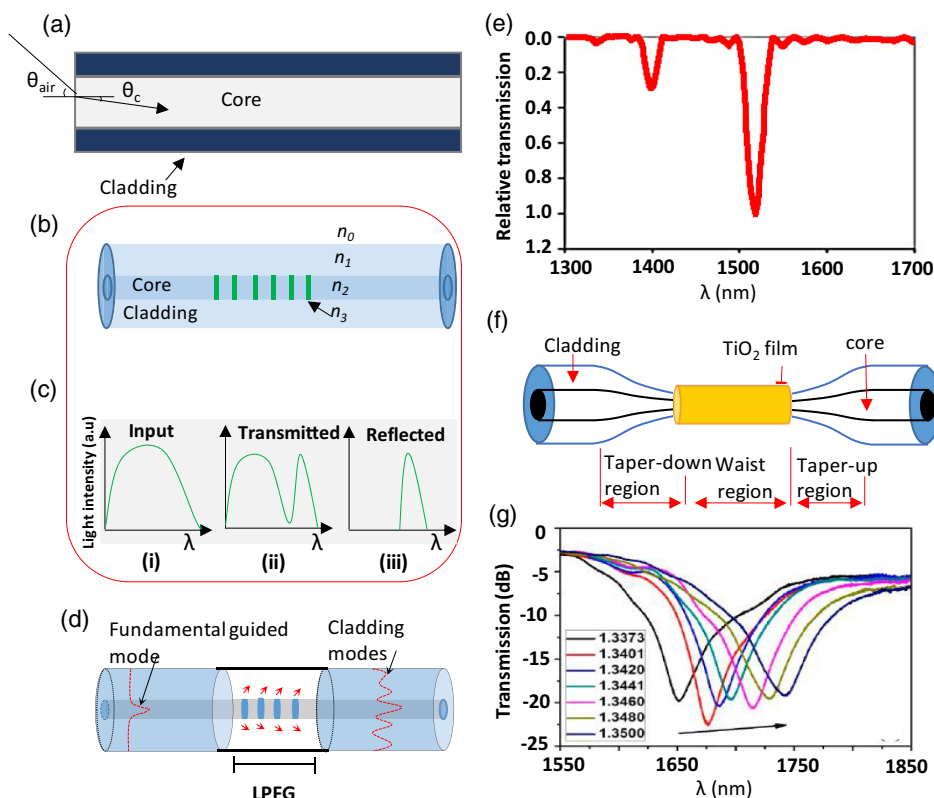


**Figure 1.** Categories of optical fibers: a) Schematic of a step-index optical fiber, b) schematic of fiber Bragg gratings, c) transmitted and reflected spectra of the light guided in a fiber Bragg grating compared to the profile of the input spectra, d) schematic of the long period grating fiber, e) transmission spectra of a long-period fiber grating showing the loss dips. Reproduced under a Creative Commons Attribution 3.0 Unported and Creative Commons 4.0 International License.<sup>[3]</sup> Copyright 2015, The Authors. Published by IntechOpen. f) Schematic of a tapered single-mode fiber where the tapered segment is covered by an analyte-responsive layer. g) Measured transmission spectra for a tapered optical fiber while the tapered section was exposed to media of different refractive indices. Reproduced under an open access Creative Commons CCBY 4.0 license.<sup>[4]</sup> Copyright 2016, The Authors. Published by MDPI.

Commonly, the single-mode fibers have a core diameter of 8–10  $\mu\text{m}$ , and are developed to function in the short infrared region. While multimode fibers are manufactured with a core diameter in the range of 50  $\mu\text{m}$  to hundreds of micrometers, and are used when high power is required to be transferred.<sup>[5]</sup> The numerical aperture (NA) of an optical fiber is the number that defines the range of angles over which the fiber can receive, guide, and release light rays. The NA of a step-index fiber is given by the difference in the refractive index between the core and cladding materials

$$NA = \sqrt{n_{\text{co}}^2 - n_{\text{cl}}^2} = n_{\text{air}} \sin \theta_{\text{air}} \quad (1)$$

where  $n_{\text{co}}$ ,  $n_{\text{cl}}$ , and  $\theta_{\text{air}}$  are the refractive indices of the core, cladding, and the incident angle of light rays, respectively. The angle,  $\theta_{\text{air}}$ , is measured relative to the longitudinal axis of the fiber core (Figure 1a).<sup>[6]</sup> Accordingly, the NA determines the range of the accepted incident angles for the light entering or exiting the fiber. A normalized frequency ( $V$ ) of optical fiber provides information about the number of optical modes that can propagate in the fiber and it depends on the NA and the core diameter. The normalized frequency is given by

$$V = (NA) \frac{2\pi a}{\lambda} \quad (2)$$

where  $a$  is the radius of the fiber core, and  $\lambda$  is the free-space wavelength.<sup>[6]</sup>

The rapid progress in developing the bio-and chemical sensors improved the healthcare systems, food, and water quality monitoring, and assisted the industry to manufacture standard products. The sensors market is still dominated by electronic sensors; however, they suffer from signal drift, and are prone to electromagnetic interference, in addition to their need for frequent calibration.<sup>[7]</sup> These limitations along with the necessity for remote monitoring/sensing directed the researchers' attention toward utilizing optical-fiber-based sensors. Using photon as the signal carrier instead of the electron, makes the optical fibers immune to the electromagnetic interferences.<sup>[8]</sup> Optical fibers serve analytical science in many ways. The fibers allow optical microscopy to be carried out over long distances reaching sites inaccessible to conventional spectroscopy.<sup>[9]</sup> In addition, optical fibers enable less common methods of interrogation such as spatially resolved spectroscopy and evanescent wave spectroscopy.<sup>[10]</sup> Optical fibers that can deliver signals with wide spectral ranges are available; however, for sensing applications, mostly long wavelengths (500 nm >) are used; as in this range the

background noise signals are weak and the lasers are used as light sources are cheap.<sup>[10]</sup> Optical fibers have been playing a significant sensing role in several fields, particularly in biomedical applications, due to their inherent advantages such as compactness, flexibility, biocompatibility, chemical inertness, and their feasibility to be machined and functionalized.<sup>[11]</sup> Furthermore, the progress in optics and photonics, chemistry, and biology enabled optical-fibers-based sensors in numerous areas including the oil and gas industry, medicine, environment monitoring, and food production. The fine dimensions of optical fibers made them suitable for integration with medical catheters and needles, which are widely used technology platforms for in vivo sensing and point-of-care diagnostics.<sup>[12]</sup> Also, their fine dimensions made them appropriate for examining small-size samples and confined remote spaces.<sup>[11b]</sup> Furthermore, they are resilient for harsh environments such as high temperature, high humidity, and dangerous atmospheres with high concentration of corrosive and explosive gases (oil/gas pipeline, oil rigs, nuclear plants), due to their robust materials and mechanical properties. In addition, optical fiber sensors can independently and simultaneously measure more than one parameter in real time and continuously.<sup>[11b]</sup>

Integration of functioning materials and structures into the optical fiber for specific sensing has been performed extensively during the past decades; however, severe limitations in their applicability have been posed due to the poor control and modest readiness to the integration methodologies. The frustration of their performance resulting from repeatability and disorder issues are obstacles to developing optical fiber technology platforms capable of competing with more mature sensing technologies.<sup>[12]</sup> Therefore, intensive research is required to adjust the fabrication technology to correctly operate on unconventional substrates such as optical fibers. In fact, most of the current micro/nanofabrication technologies arising from the microelectronic industry have been made to operate on planar substrates; however, they are not convenient for optical fibers because of fibers' small cross-section and curved surfaces.<sup>[12]</sup> Recently, intensive research has led to the development of crucial fabrication routes allowing fine control of process parameters at nanoscales. The recently developed nanotechnologies and self-organization methods used for patterning and depositing materials have been successfully applied to optical fiber sensing platforms.

Several reviews have been published in the past few years covering optical fiber sensors. Each of these reviews addresses either a specified category of optical fiber sensors and its possible applications or the detection of a specified parameter by numerous categories of optical fiber probes.<sup>[7,11b,12,13]</sup> However, this review covers many categories of fiber-optic sensors presenting the foundation of chemical and biosensing, including the sensing mechanism, sensing materials, and the strategies for improving the sensors' performance. Additionally, the recent developments in optical fiber sensors are summarized, analyzed, and discussed. Furthermore, this review addresses the light-diffuser-integrated optical fiber sensors, which have not been addressed in the previous reviews, to the best of the authors' knowledge. Finally, a conclusion along with examples of the fiber sensing technologies that reached the market and the market expectation are provided. The aim of this review is to bring the attention to the potential applications of the fiber-optic sensors based on

different sensing mechanisms – giving the reader a wide overview of the feasible applications in the biomedical, industrial, and environmental fields. Also, the review provides an overview of the physical/chemical phenomena synergistic with optical fibers for sensing purposes, with more attention paid to biomedical applications. The review is structured as follows: the introduction addresses the simple basics of optical fibers and the advantages of utilizing fiber optics in sensing applications introducing the readers into the field. The next sections describe in detail the different fiber optic sensors which are classified according to the physical/chemical phenomena integrated with the fiber-optic for developing the sensors. The distributed optical fiber sensors, photonic crystal fibers, and those based on specklegrams are not involved in this review. For readers interested in the unaddressed fiber sensors, there are several recent reviews that address them.<sup>[14]</sup>

## 2. Fiber Bragg Gratings (FBGs)

FBGs is a traditional fiber that combines a distributed Bragg reflector fabricated in a short segment of the fiber core to reflect a specific wavelength range of the guided modes and transmits all others (Figure 1b,c). Bragg reflector is a periodic variation in the refractive index of the fiber core in the guidance direction, and functions as a wavelength-selective dielectric mirror.<sup>[15]</sup> Electromagnetic waves propagating through FBGs are transmitted except for the wavelengths that satisfy Bragg's law, which is reflected. The simplest configuration of FBGs is the uniform grating, in which the refractive index modulation has a constant period along the grating segment. The reflected spectrum by this standard FBGs shows a peak centered around the Bragg's wavelength, with reflectively 10% and 90% for FBGs having length ranges of 3 mm and 10 mm, respectively.<sup>[16]</sup> And the reflected bandwidth is 0.03 nm for FBGs operating at 1550 nm. A more complicated FBG called chirped FBG (CFBG) is defined by a non-uniform modulation of the grating period. For the linear CFBG, the periodicity constant increases at a constant rate through the grating segment. Consequently, the CFBGs do not diffract a single wavelength but the reflected spectrum shows a broad bandwidth; as each sub-segment of the grating diffracts/reflects a different Bragg's wavelength. Readers interested in CFBGs are referred to the cited review articles.<sup>[13n]</sup>

Initially, FBGs were developed for the telecommunications industry in the 1990s, later, FBGs were incorporated into sensing applications. The principle by which FBGs are used in sensing is based on detecting the shift in the Bragg gratings wavelength, which occurs due to a change in the grating period or the effective refractive index ( $n_{\text{eff}}$ ). Advantageously, FBGs can function in both transmission and reflection configurations. The reflection configuration does not require both ends of the fiber to be connected to the interrogation setup – making this mode more practical. Insensitivity of the FBGs to the fluctuation of the illumination intensity of the light source is another merit as the output signals are obtained by recording the wavelength shift induced by the measurand. FBGs probes were utilized for temperature, humidity, strain, and infrared radiation detection.<sup>[15,17]</sup> For instance, an FBGs probe was developed for temperature detection based on the thermo-optic effect of the fiber's core

material induced by the temperature. The Bragg gratings were fabricated in a single-mode silica fiber with a grating period of 1.55  $\mu\text{m}$ .<sup>[17b]</sup> Recently, polymer FBGs were utilized for detection of the relative humidity in ultra-high performance concrete mixture for eight hours continuously.<sup>[18]</sup> FBGs were used for pH sensing applications too. Multilayers of PVA/PAA were deposited on FBGs by the dip-coating method for developing a pH sensor.<sup>[19]</sup> The hydroxyl groups of PVA and the carboxyl groups of PAA were cross-linked by heating up the multilayers. The fiber sensor showed a linear response to pH in the range of 3–7, presenting a sensitivity of 0.0122 nm pH<sup>-1</sup> resulting from the change of the swelling degree of the hydrogel in different pH conditions. Good repeatability was observed; however, the response time was too slow and lasted several minutes. In a similar study, the FBGs was functionalized with poly(ethylene glycols), sodium alginate, and poly(N-isopropylacrylamide) for a wide range sensing of pH.<sup>[20]</sup> The response time was improved reaching 1.33 min and the sensor working range was extended to cover whole the pH range (0–14). However, the sensor's response was nonlinear and the sensitivity was very low. Metal ions, such as calcium, potassium, sodium, and magnesium, exist in high abundance in most biological organisms, and also some heavy metal ions are essential in our bodies but existed in small quantities. However, heavy metal ions are harmful and fatal when existed in amount exceeding a certain range. For example, increasing amounts of Cr<sup>+3</sup>, Cd<sup>+2</sup>, Cu<sup>+2</sup>, and Ni<sup>+2</sup>, may cause skin, bone, and teeth diseases.<sup>[21]</sup> FBGs have become a versatile tool for measuring trace amounts of ions. For instance, trace amounts of Cr<sup>+6</sup> ions were detected by FBGs where tetraalkylammonium salts containing poly(3-arylamidopropyltrimethylammoniumchloride) hydrogel was dip-coated on the surface of the grating area.<sup>[22]</sup> Complexation of the Cr<sup>+6</sup> ions with the hydrogel led to swelling of the hydrogel changing the diffracted wavelength. The sensor presented a linear response in the concentration range of 10–100 ppb.

The industrialization made the whole world face severe gaseous pollution problems which affect people's daily life. Reliable gas sensors may play a significant role in environmental monitoring applications. Hydrogen gas was found to cause explosion when its concentration reaches 4–74.5%.<sup>[23]</sup> Thus, it is essential to monitor H<sub>2</sub> for ensuring safe work conditions. For instance, FBGs were coated with a palladium layer for hydrogen sensing application.<sup>[24]</sup> Palladium is a well-known catalyst for H<sub>2</sub>, which dissociate H<sub>2</sub> into atomic hydrogens and shows a strong affinity to dihydrogen.<sup>[25]</sup> Adsorption of the H<sub>2</sub> on the Pd film induced a change in the refractive index of the Pd layer. The working window of the fiber sensor was in the range of 0.3–1.8%, which is lower than the lowest critical explosion concentration of the H<sub>2</sub>. Also, the FBGs were developed for smart structure applications. The FBGs were embedded into the structures to monitor the strain distribution.<sup>[26]</sup> The latter is valuable as the real-time monitoring of structures assists in improving the safety of the structures because it allows timely repair and prevents unwanted damages.<sup>[27]</sup> A deflection and twist measuring method applicable for ground and flight tests was developed based on FBGs.<sup>[28]</sup> The left-wing of a Global 7500 business jet was instrumented with the FBGs and underwent a durability and damage tolerance certification test. The optical fiber system

allowed distributed strain measurements on the wing, and consequently the aircraft wing deflection.

To exploit the FBGs in biosensing applications, two configurations have been introduced. The first method is to manufacture tilted FBGs, in which the refractive index modulation plane is tilted with respect to the longitudinal axis of the fiber by angles lower than 10°. This tilted grating has a similar diffractive wavelength to the standard FBG but it excites several cladding modes at the interface between the cladding and the outer medium. These modes are detected in reflection by coating the fiber tip with a reflecting layer such as gold and the modes appear as a comb of narrow linewidths at wavelengths smaller than the Bragg's wavelength. For instance, a tilted FBGs probe was introduced for selective glucose detection based on an enzyme immobilized on the cladding of the FBGs. The probe showed a sensitivity of 0.298 nm mm<sup>-1</sup> as the Bragg wavelength shifted only 1 nm over the change in glucose concentration in the physiological range.<sup>[29]</sup> Tilted FBGs were developed for pH sensing based on a pH-responsive multilayer hydrogel (poly(diallyldimethyl ammonium chloride/PAA).<sup>[30]</sup> The developed fiber showed a reasonable sensitivity of 0.5 nm pH<sup>-1</sup> and a rapid response of 10 s. Also, tilted FBGs were reported for lead detection based on black phosphorus (BP).<sup>[31]</sup> The BP nanosheets were synthesized using the liquid-phase exfoliation method and the in situ layer-by-layer technique. The fiber sensor was tested for heavy metal ions detection (Pb<sup>+2</sup>), and demonstrated high sensitivity of 0.5 × 10<sup>-3</sup> dB ppb<sup>-1</sup>, limit of detection of 0.25 ppb, and functioning window of 0.1–1.5 × 10<sup>7</sup> ppb.

The second strategy for enhancing the performance of the FBGs is to chemically etch the cladding of the FBGs segment. In this case, the poor light confinement in the fiber core causes a change in the effective refractive index with the outer medium. As a result, Bragg's wavelength and the light intensity shift when the grating is exposed to outer media of different refractive indices. For example, etched FBGs were used for pH sensing applications by functionalizing the fiber with poly-allylamine hydrochloride and poly-acrylic acid (PAH/PAA) multilayer, which was deposited by the layer-by-layer electrostatic-self-assembly technique.<sup>[32]</sup> In this method, the sensitivity of the sensor significantly improved to reach 0.64 nm pH<sup>-1</sup> which was one order magnitude higher than the commonly used FBGs for pH sensing developed based on the same pH-responsive hydrogel. Also, a palladium film of thickness of 150 nm was deposited on a tapered FBG to develop a hydrogen sensor.<sup>[33]</sup> Compared to the traditional FBGs sensor based on the Pd layer, the fiber sensor showed a significantly enhanced sensitivity of 81.8 pm/%v/v H<sub>2</sub>. Also, an etched FBGs probe was reported for sensing glucose and C-reactive proteins.<sup>[34]</sup> Sridevi et al. etched a single-mode fiber that was FBGs-inscribed, and coated the fiber with aminophenylboronic acid (4APBA)-functionalized RGO complex.<sup>[34a]</sup> The 4APBA played the role of glucose-recognition agent and complexed with glucose, resulting in a shift in the Bragg's wavelength. The fiber showed a linear response trend with glucose concentration in the range of 1 nM–10 mM, showing a limit of detection of a 1 nM. FBGs recently reported for monitoring breathing patterns and respiratory rates.<sup>[35]</sup> The clinical test was performed on nine volunteers, and showed a competitive performance to the spirometer in detecting the respiratory rates.

By etching the FBGs, the effective refractive index of the fundamental fiber propagating mode shows a non-linear dependence on the external refractive index. For the nonuniform FBGs, its spectral response is strongly modified leading to the split of the Bragg wavelength into two sub-peaks. The peak related to the etched grating region depends on the etching features, surrounding environment, and the local temperature. The second peak is related to the unperturbed grating region (cladding covered) which is sensitive only to local temperature. The maximum sensitivity for the surrounding refractive index is achieved when the cladding layer is completely removed during the etching and the surrounding refractive index is close to the cladding. The nonuniform FBGs were demonstrated for simultaneously monitoring the refractive index change and temperature. For instance, Iadicicco et al. demonstrated nonuniform FBGs for self-temperature compensated refractive index measurements.<sup>[36]</sup> A standard fiber Bragg grating was partially or totally etched along half of the grating segment. Changing the surrounding refractive index led to splitting the reflected wavelength into two peaks: a peak at shorter wavelengths corresponding to the etched region which responds to both the local refractive index and temperature, and the second peak is located at longer wavelengths responding only to temperature changes. The simultaneous detection of the Bragg wavelengths related to etched and un-etched grating regions provided accurate measurements of the refractive index and temperature by using a single sensing element. In another study, the wet chemical etching in hydrofluoric acid was used to completely remove the cladding surrounding the grating segment in a single-mode fiber (SMF-28).<sup>[37]</sup> The fiber detected the surrounding refractive index in the range of 1.333–1.450. Iadicicco et al. developed nonuniform FBG for simultaneous detection of temperature and refractive index. The working window for the developed sensors was in the refractive index range of 1.33–1.45 when the temperature varied in the range of 15–50 °C. In this study, the cladding was partially removed where only 7.6 μm of the cladding thickness was left.

The fabrication process of the FBGs is relatively complex and requires advanced systems such as laser interference system and femtosecond lasers. The fabrication process is commonly carried out by: 1) laser interference, in which two coherent beams are used to create the desired grating period; 2) phase mask technique, in which a quartz glass with a fixed corrugated surface is used for UV inscription of the gratings; or 3) point-by-point technique, in which a femtosecond laser is used for fabricating the gratings producing a groove per a laser pulse.<sup>[17a]</sup> High-resolution spectrometers are required in the interrogation setup of the FBGs probes, which make the device bulky. Typically, FBGs probes are interrogated by a rapid scanning tunable laser coupled to a three-terminal coupler at the one-fiber end, and a spectrometer coupled to the reflection terminal of the three-terminal coupler, and the other end of the FBGs is left free. This system allows to detecting the reflected spectrum, and by using a peak-tracking technique, Bragg's wavelength is accurately detected. Some applications of the FBGs, especially in the biomedical field, have been dampened by the necessity for both a tiny interrogation unit and a convenient physical connection between the interrogator and the FBGs. However, recent steps have been taken forward to curb the interrogator bulkiness

and the related costs. Currently, miniaturized interrogation system with dimensions of 40 × 40 × 50 mm and cost \$7000 are available. But improving the performance of the miniaturized interrogators is still an open challenge since they provide lower resolution, lower integration speed, narrower wavelength bandwidth, and fewer channels as compared to the bulky interrogators. Another limitation of the FBG probes is that the probes are sensitive to temperature and strain, which represent a challenge when an FBG is employed for detecting other measurands. Once the aforementioned challenges are addressed, the next generation of FBGs portable probes will be realized.

### 3. Long-Period Fiber Grating (LPFG)

An LPFG is a traditional fiber involving a structure that has a periodic modulated refractive index similar to that of the fiber Bragg gratings (Figure 1d). However, the period is larger, on the millimeter scale, which makes the fabrication process relatively simpler. The period of the LPFG exceeds the wavelength of the electromagnetic waves guided in the fiber as the grating period is in the range of 0.1–1.0 mm and has a length of a few centimeters.<sup>[38]</sup> In contrast to the FBGs, the LPFG is a transmission mode fiber, as it shows no backward reflection, and isolation is not required in the sensing system.

The LPFG has been developed and improved for decades, which resulted in numerous fabrication techniques and sets of different sensor types: from simple LPFG, interferometric systems, plasmonic-based sensing, to special fibers such as photonic crystals. The LPFG can be manufactured in optical fibers by irradiation with an ultraviolet (UV) source, laser source, mechanical pressure, and electric arc discharges.<sup>[38]</sup> In 1996, the first long-period gratings were inscribed in optical fiber for band rejection applications. Since then, LPFG has been developing for optical communications and optical sensing systems. In optical communication systems, LPFG has been employed as gain equalizing filters, wavelength selective devices, and band pass and band rejection filters. In the same year, the first LPFG probe was also introduced for sensing applications.<sup>[39]</sup> The LPFG-based sensors were applied for structural bending, temperature, strain, refractive index, and biochemical sensors.<sup>[40]</sup> In the long period grating segment, the core guided modes couple with those modes propagating forward in the cladding. The LPFG segment takes away the core wavelengths of phase coincident with its periodic constant. Therefore, these wavelengths are observed in the transmission spectrum as loss dips (Figure 1e). The coupling wavelengths are given by the phase-matching condition

$$\lambda_m = (n_{\text{eff,co}} - n_{\text{eff,cl}}^m)\Lambda \quad (3)$$

where  $\lambda_m$  is the wavelength of the  $m^{\text{th}}$  cladding mode,  $\Lambda$  is the grating period,  $n_{\text{eff,co}}$  is the core effective refractive index, and  $n_{\text{eff,cl}}^m$  is the effective refractive index of the  $m^{\text{th}}$  cladding mode.<sup>[39]</sup> The transmission of the resonance wavelength in the LPFG is given by

$$T = \cos^2(D_c I_g / 2) \quad (4)$$

where  $I_g$  is the grating length and  $D_c$  is the coupling coefficient. If the LPFG segment of a fiber is exposed to an external stimulus

that is capable of modifying either  $n_{\text{eff,co}}$ ,  $n_{\text{eff,cl}}^m$ , or  $\Lambda$ , it causes a shift in the loss/dip wavelengths according to the coupling equation. Biosensing/biomedical applications are based on modifying the effective refractive index of the cladding by coating the LPG segment with an analyte-responsive layer. Changing the refractive index of the responsive layer induces a change in the resonant wavelengths.<sup>[41]</sup> For example, an LPG was fabricated in a single-mode fiber using a laser technique for selective glucose detection.<sup>[42]</sup> The LPG had a periodicity of 0.55 mm and was silanized to secure binding sites for immobilizing the glucose-recognition agent, glucose oxidase. The change in the refractive index of the outer coating occurred due to glucose-enzyme binding, which led to a shift in the resonance wavelengths that were detected in the transmission spectra. The resonance wavelength shifted by 2 nm over the change of glucose concentration in the physiological range (4–8 mM), which reflects the poor sensitivity of the fiber. In general, the sensitivity of the LPFG for refractive index changes in the surrounding environment is relatively low,  $\approx 700 \text{ nm RIU}^{-1}$ , and for biosensing applications the sensitivity must be enhanced to reach  $1000 \text{ nm RIU}^{-1}$ . One of the approaches to increase the sensitivity is to induce coupling to the higher order cladding modes resulting in the phenomenon of dual resonance. In this case, the same cladding mode is excited at two distinguished wavelengths. The latter phenomenon doubles the sensitivity of the LPFG-based sensors. The second approach to enhance the sensitivity is to use nano/microstructures such as graphene oxides. For instance, a higher glucose-sensitive LPFG probe was reported based on graphene oxide-glucose oxidase (GOD) via the chemical crosslink method.<sup>[43]</sup> The graphene oxide layer was coated on the LPFG segment to immobilize glucose oxidase through its binding sites. The reaction of glucose and GOD generates gluconic acid and hydrogen peroxide led to an increase in the surrounding refractive index. The probe showed a linear response with a sensitivity of  $0.77 \text{ nm (mg mL)}^{-1}$ . Recently, applications of the LPFG in the biomedical field extended to virus detection. For instance, norovirus which is the main cause of acute gastroenteritis was detected of quantity  $1 \text{ ng mL}^{-1}$  in a 40 min assay.<sup>[44]</sup> The detection was carried out by an LPFG coated with antibodies and protein of norovirus. More recently, the LFBG was reported for C-reactive protein detection in serum.<sup>[45]</sup> The LPFG was coated with graphene oxide to provide functional groups for covalently immobilizing the biological recognition element (anti-CRP). The probe showed a very low LOD of about  $0.15 \text{ ng mL}^{-1}$  for the CRP and a wide working range of  $1 \text{ ng mL}^{-1}$ – $100 \text{ }\mu\text{g mL}^{-1}$ .

LPFGs offer a number of advantages such as low insertion losses, and relatively higher sensitivity to the surrounded refractive index changes as compared to FBGs. In addition, LPFG has the potential to be endowed with different degrees of complexity: from single grating to applications in numerous sensing fields using enhancing techniques such as mirror ends and tapered LPFG. Furthermore, the resonance wavelength of the LPFG can be easily tuned anywhere in the electromagnetic spectrum including the infrared region. However, LPFG requires a relatively complex fabrication process which is usually carried out using a laser source, mechanical pressure, electric arc discharges, or UV light source.<sup>[38]</sup> Also, as in the case of FBGs, bulky and costly instruments such as a spectrometer and computer are

necessary for reading out the sensor. Additionally, the LPFG suffers from poor mechanical properties in the zone where the long grating segment is located. Interference of temperature and strain in biosensing applications is another concern, which is due to that the fiber's core itself is made of a temperature-sensitive material. Furthermore, LPFG offers a low Q-factor due to the broad resonant wavelength band which decreases its limit of detection.<sup>[29]</sup>

#### 4. Tapered Optical Fiber Interferometer (TOFI)

A TOFI is a traditional optical fiber stretched out over a small length to create a region of a very thin diameter called neck (Figure 1f). In traditional fibers, light is guided in the fiber core but a minute portion of the light energy (evanescent waves) penetrates the fiber cladding.<sup>[46]</sup> These evanescent waves decay exponentially into the cladding with a penetration depth

$$d_p = \frac{\lambda}{2\pi\sqrt{n_{\text{co}}^2 \sin^2 \theta_i - n_{\text{cl}}^2}} \quad (5)$$

where  $\theta_i$  represents the incident angle of the light rays at the core-cladding interface,  $n_{\text{co}}$  is the fiber core refractive index,  $n_{\text{cl}}$  is the cladding refractive index.<sup>[46]</sup> Tapering a single-mode fiber decreases the V-number of the core to be less than one due to the decrease in the fiber core radius. However, the cladding V-number increases above 2.405; as a result, the light is no longer guided by the fiber core – spreading to the cladding that starts to play the role of the new core. The refractive index difference between the cladding and the surrounding medium guides modes in the tapered region and the new V-number is given by

$$V_{\text{cl}}(z) = \frac{2\pi a(z)}{\lambda} \sqrt{n_{\text{cl}}^2 - n_{\text{ex}}^2} \quad (6)$$

where  $a(z)$  and  $n_{\text{ex}}$  are the radius of the fiber waist and the RI of the external medium.<sup>[47]</sup> Thus, the tapering creates a region where the external surrounding medium plays a role in guiding the fiber modes. Also, the penetration depth of the evanescent waves in the tapered segment depends on the RI of the surrounding medium and is given by<sup>[48]</sup>

$$d_p = \frac{\lambda}{2\pi\sqrt{n_{\text{cl}}^2 \sin^2 \theta_i - n_{\text{ex}}^2}} \quad (7)$$

In sensing applications, stimuli-responsive layers are coated on the tapered segments to be the external surrounding media. The refractive index of the analyte-responsive layer changes due to its response to a certain analyte – inducing a change in the intensity of the transmitted light. Therefore, measuring the variation in the transmitted light is correlated to the refractive index of the responsive-coating layer, and consequently the analyte's concentration (Figure 1g). For instance, a single-mode silica fiber was tapered and functionalized at the tapering segment for bacterial growth detection.<sup>[46]</sup> The fiber was tapered by a CO<sub>2</sub> laser under an applied tension and the tapering process was monitored by an optical microscope. A laser source with wavelength

and power of 1558.17 nm, and 20 mW, respectively, illuminated the fiber and the transmitted optical signals were collected at the other end of the tapered fiber by a photodetector—and the bacterial growth rate was detected at room temperature. Chen et al. developed a tapered single-mode fiber for *Staphylococcus aureus* (*S. aureus*) detection based on pig immunoglobulin G (IgG) as a recognition agent.<sup>[49]</sup> The probe showed a maximum wavelength shift of 2.04 nm for *S. aureus* concentration of  $7 \times 10 \text{ CFU mL}^{-1}$ , and a response time of 30 min.

Also, multimode fibers were tapered for biosensing applications. For example, a multimode polymer fiber made of poly(methyl methacrylate) was developed for glucose sensing.<sup>[50]</sup> The tapered segment of the fiber was 1.5 cm long and was coated with a single layer of graphene. Introducing the aqueous glucose solution into the tapered region caused a change in the RI of the fiber surrounding medium, which influenced the evanescent field resulting in a change in the fiber transmitted signals. The fiber showed low sensitivity which limited its application for glucose detection under physiological conditions. The interrogation setup combined a light-emitting diode (628 nm) as a light source along with a constant current power supply, convex lenses to focus the light entering the fiber, light polarizer, and a spectrometer. Recently, tapered optical fiber was applied for detecting the dissolved oxygen based on the layer-by-layer self-assembly process used to deposit the oxygen-sensitive fluorescent dye onto the surface of the tapered region.<sup>[51]</sup> The probe showed a response time of 88 s along with repeatability and temperature stability. Deng et al reported a tapered fiber for head and neck cancer screening.<sup>[52]</sup> Interleukin-8 (IL-8) as a biomarker for head and neck squamous cell carcinoma (HNSCC) was detected by attaching a molecular recognition agent to the tapered segment of the optical fiber. A tunable fiber laser illuminated the tapered fiber from one end and the intensity of the transmitted light at the other end was recorded by a spectrophotometer and the biomarker concentration  $10 \text{ pg mL}^{-1}$  was detected.

However, tapered fibers allow access to the evanescent waves of the propagating modes which are beneficial for chemical/physical/biological applications. There are many challenges still open such as the complex fabrication process, low sensitivity, influence of the intensity modulation of the light source, poor mechanical properties, and the complexity of the interrogation setup. For many applications which require carrying out the test in reflection configuration, the TOFI isn't convenient. For example, the TOFI is not appropriate for implantable sensors for biomarkers detection.

## 5. Interferometric Fiber-Optic Devices

Fiber-optic interferometers are based on the interference which occurs between two light beams propagating through different optical path lengths (OPLs) in the same optical fiber or in two different fibers. The interferometric fiber consists of a light beam splitter and a light beam combiner in any configuration.<sup>[53]</sup> In sensing applications, one of the optical path lengths is configured to be influenced by the external perturbations. The interferometric fiber detects quantitatively the perturbation by presenting a change in the wavelength, phase, intensity, frequency, or bandwidth.<sup>[54]</sup> Currently, the trend of the interferometric optical

fibers is the miniaturization for microscale applications; hence, bulk optical components such as objective lenses, beam splitters, and beam combiners are replaced by small parts to develop simple and compact fiber probes.<sup>[13e]</sup> Interferometric fiber-optic sensors are classified into four categories: tapered fiber interferometer, Fabry–Pérot, Mach–Zehnder, Michelson, and Sagnac.<sup>[13e]</sup>

### 5.1. Fabry–Pérot Interferometer Fiber (FPIF)

The FPIF is a traditional optical fiber that has two parallel reflecting surfaces isolated by a certain distance.<sup>[55]</sup> The reflecting surfaces can be constructed inside or outside the fiber, and based on that the FPIFs are classified into two groups: intrinsic and extrinsic (Figure 2a,b).<sup>[56]</sup> The transmission and reflection spectra of an FPIF depend on the optical phase difference (OPD) between the two interfering light beams. The spectrum of an FPIF displays crests and dips which refer to that both beams of that particular wavelength being in phase or out of phase. The optical phase difference of the FPIF is given by

$$\delta = (2\pi/\lambda_0)2nL_c \quad (8)$$

where  $\lambda_0$  refers to the wavelength of the free-space incident light,  $n$  represents the refractive index of the cavity material, and  $L_c$  refers to the length of the cavity.<sup>[13e]</sup> Any perturbation that occurs in the cavity region of the FPIF induces a change in the OPD. Consequently, the transmission and reflection spectra are modified. If an applied longitudinal strain on the fiber altered the cavity length or the refractive index, the OPD shifts. By detecting the change in the transmission or reflection spectrum of the FPIF, the applied strain is detected.<sup>[57]</sup>

For biosensing applications, FPIF probes based on stimuli-responsive hydrogels have been developed.<sup>[58]</sup> The cavity was made of an analyte-responsive polymer and attached to the fiber tip constituting an extrinsic FPIF. The fiber's core–polymer and the polymer–environment interfaces represent the reflecting mirrors/surfaces. The Fresnel reflected beams from these interfaces generate the interference fringes that appear in the reflection spectrum. Upon changing the refractive index or the length of the responsive-polymer cavity, the OPD changes, and accordingly the pattern of the interference fringes. For instance, a Nafion film which is sensitive to humidity, was deposited on the fiber tip forming an extrinsic Fabry–Pérot cavity (Figure 2c). Upon absorption of water vapor by the Nafion film, its refractive index and thickness/length changed – inducing an OPD shift, and consequently a change in the interference fringes of the recorded spectrum.<sup>[58a]</sup> Similarly, a thin film of cellulose acetate butyrate was deposited on a fiber tip constituting a Fabry–Pérot cavity for humidity sensing.<sup>[58b]</sup>

In a trial to eliminate the necessity for the high-quality responsive-films required in the Fabry–Pérot fiber sensors, a half-sphere shape of a pH-responsive-hydrogel was attached to the end of an optical fiber (Figure 2d). The radius of the half-sphere was 50–60  $\mu\text{m}$ . The fiber probe was able to detect the change in the radius of the hydrogel with a precision of 2 nm.<sup>[58c]</sup> This configuration for the FPIF probe eradicated the necessity for high-quality films. However, two constraints emerged: 1) the refractive index difference between the bound

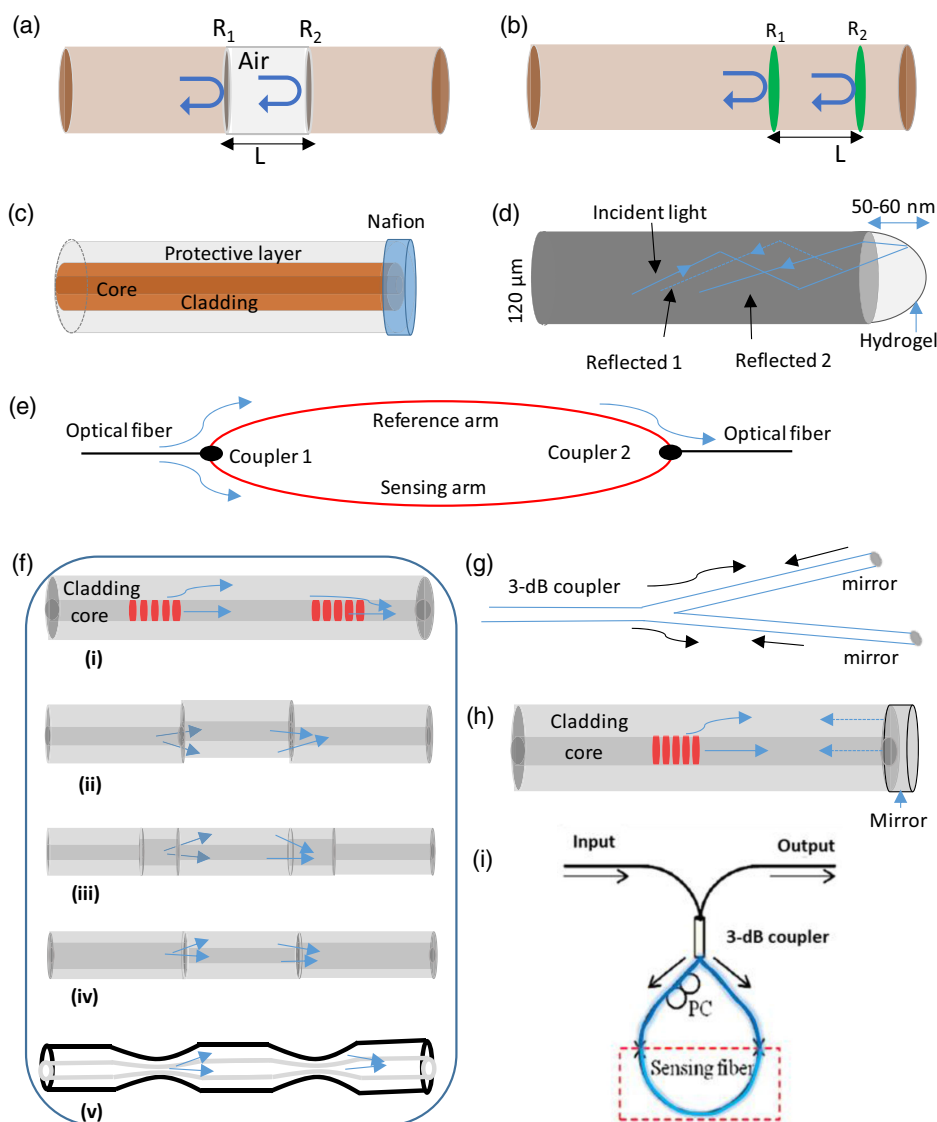


**Figure 2.** Categories of interferometric optical fiber probes: a) An extrinsic Fabry–Pérot interferometric (FPI) fiber having an external air cavity, b) An intrinsic FPI fiber having two reflecting surfaces along the fiber, c) FPI fiber used for humidity sensing, the probe made of a high-quality film deposited on the fiber tip constituting the external cavity, d) FPI fiber, the cavity made of pH-responsive hydrogel having a half-sphere shape, e) the Mach–Zehnder fiber interferometer. f) Various configurations of in-line MZIs based on: i) a pair of LPGs, ii) mismatching of fiber cores, iii) multimode fiber segment, iv) single-mode fiber between two multimode fiber segments, v) two tapered regions. g) The initial configuration of the Michelson interferometer. h) In-line configuration of Michelson interferometer fiber-based on an LPG. i) Sagnac interferometer. Reproduced under an open access Creative Commons CCBY 4.0 license.<sup>[13e]</sup> Copyright 2012, The Authors. Published by MDPI.

hydrogel and the environment must be significant to enable high reflectivity at this interface, which put constraints on the selected monomer and cross-linker concentrations; and ii) depositing the polymer on the fiber tip in the form of a half-sphere was a challenge because the gel droplet doesn't retain the spherical shape during the polymerization.<sup>[58c]</sup> FPIF probes for glucose sensing were developed based on the same configuration.<sup>[58d,59]</sup> The probe presented a high sensitivity, low limit of detection, and short saturation time ( $\approx 20$  min) under the conditions pH of 7.4 and temperature of 37 °C. Coherent light sources used in FPIF probes increase the cost of the probe's setup. To eradicate

the necessity for coherent light sources, a multilayer of a pH-responsive hydrogel was deposited on the fiber end building up a Fabry–Pérot nanocavity by using the electrostatic self-assembly technique. A low-coherent light source, a halogen lamp of illumination wavelength 950 nm was coupled to the fiber probe for pH detection.<sup>[60]</sup> Recently, the FBIF probe was reported for low-pressure measurements for industrial applications.<sup>[61]</sup> The FPIF probe was able to detect the pressure in the range of 5–50 mBar with maximum and average errors of 3.77% and 1.45%, respectively. For high-pressure sensing (40 MPa), a silica diaphragm was attached to the optical fiber end, and its



thickness was precisely controlled by the fiber tip polishing technique.<sup>[62]</sup> The sensitivity was enhanced significantly by reducing the thickness of the silica diaphragm. High sensitivity of  $1.436 \text{ nm MPa}^{-1}$  was demonstrated in the pressure range of 0–40 MPa at the diaphragm thickness of 4.63 nm. For temperature sensing application, a solid film of DNA was deposited on an optical fiber's end constituting the exterior FBI.<sup>[63]</sup> Based on the thermo-optical properties of the DNA layer, the probe showed high-temperature sensitivity of  $2.42 \text{ nm } ^\circ\text{C}$  in the temperature range of 30–80 °C.

FBI probes are very promising among the numerous emerging optical fiber sensors as they offer immunity to environmental noise, are simple, versatile, and responsive. Also, the FBI probes allow for accurate in situ measurements in regions hard to reach; however, there are some challenges still open. The complexity of fabrication is one of these challenges, which has limited their commercial growth.<sup>[64]</sup> Additionally, the FBI probes require high-quality films and coherent light sources, which add an extra cost to the sensor. Furthermore, the readout setup requires bulky instrumentations such as computers to process the output signals.

## 5.2. Fiber-Optic Mach–Zehnder Interferometer (FOMZI)

Early designs of FOMZI combined two independent fibers which function as a reference and sensing arms. The FOMZI consists of an optical fiber that guides the light to a splitter, so light enters the reference and sensing arms; the light is then recombined to be guided through another optical fiber reaching the photodetector (Figure 2e).<sup>[13e]</sup> The recombined light presents interference fringes that depend on the optical path difference between the arms. For remote sensing applications, the sensing arm is exposed to the tested analyte, and the reference arm is kept isolated. The analyte influences the sensing arm inducing a change in the optical path difference.<sup>[13e]</sup>

The configuration of FOMZI which is based on the two separate fiber arms was replaced with an in-line interferometer by introducing the long-period grating (Figure 2f). The LPG acts as the light splitter and the light combiner. The guided beam in a single-mode fiber (SMF) is split by an LPG into two modes: core and cladding, and both modes are recombined by another LPG-originating interference fringes.<sup>[65]</sup> The FOMZI probes based on a pair of LPGs have limited operation wavelengths as the LPG functions in limited ranges of wavelengths because of the phase-matching phenomenon of the gratings. Additionally, the LPG pair in the FOMZI has to be identical to achieve maximum performance.<sup>[66]</sup> Therefore, alternative methods have been used to split the core-guided modes into core and cladding modes. For instance, two fibers can be spliced with a minute lateral offset (Figure 2f–ii). The offset makes part of the core mode split into cladding modes and core modes, and recombines them on the other side. This type of FOMZI is less costly and can be fabricated rapidly as compared to the LPG-based FOMZI. Also, it does not suffer from the limitation of the narrow band working wavelength.<sup>[13e]</sup> Tapering the optical fiber at two points can construct an effective in-line FOMZI too (Figure 2f–v). The core mode splits at the first point into core mode and cladding mode; both modes recombine at the second

tapering point originating interference fringes. Although this type of FOMZI is compact, it suffers from weak mechanical regions (tapered zones).<sup>[13e]</sup> Figure 2f shows the other possible methods employed for splitting the core-guided mode.

FPMZI probes have been employed for detecting temperature, humidity, strain, and gases as the sensitivity of the cladding modes to the refractive index of the surrounding medium was identified.<sup>[65c]</sup> For instance, an in-line FOMZI probe based on long-period gratings was demonstrated for ammonia gas sensing.<sup>[67]</sup> The fiber was coated with graphene that absorbed ammonia molecules and gave rise to a shift in the interference spectrum with an amount depending on ammonia concentrations. The probe showed a sensitivity of  $3 \text{ pm ppm}^{-1}$  for the ammonia concentration range of 10–180 ppm. Also, Fan et al developed the FOMZI probe for humidity sensing based on graphene oxide as a responsive material.<sup>[68]</sup> The refractive index of the deposited graphene oxide changed due to the absorption of the water molecules and consequently, the resonant dip shifted with the ambient relative humidity. The probe showed a sensitivity of 0.19 and  $0.061 \text{ nm}/\% \text{RH}$  in the relative humidity range of 30–55% and 55–95%, respectively.

In general, FOMZI is a transmission type interferometer, so sensors based on this type of interferometer can't achieve plug-in measurements which is a major hindrance to the application of such sensors in many fields, including in vivo measurements.

## 5.3. Fiber-Optic Michelson Interferometer (FOMI)

The working principle of the FOMI is analogous to FOMZI.<sup>[13e]</sup> The guided light in the fiber core is split to propagate in reference and sensing fiber arms. However, the guided light is reflected at the end of each arm by mirrors to recombine in the light launching fiber. Thus, the main difference compared to FOMZI is the terminal reflectors, which provide the FOMI the advantage of working in the reflection configuration (Figure 2g). FOMI is compact, handy, and practical in use and installation because it functions in reflection mode. Multiplexing possibility with parallel connectors of several sensors is another advantage of the FOMI probes. However, adjusting the difference in the fiber length between the sensing fiber arm and the reference fiber arm with the coherent light source is essential. An in-line configuration of the FOMI was developed based on a single LPG fabricated in a cladded fiber (Figure 2h). The LPG divides the guided mode into two paths representing the two arms of FOMI. The light in each path is reflected by a mirror manufactured on the fiber's end and the reflected light recombines in the core by the same LPGs – giving rise to interference fringes in each resonance band.<sup>[69]</sup> In-line FOMI was developed for refractive index sensing as the interference fringes and its intensity shifted with increasing the refractive index.<sup>[69a]</sup> The fringes' positions shifted 55 nm upon increasing the refractive index of the aqueous solution in the range of 1.33–1.44. Other applications for the FOMI were also reported. For instance, Dong et al. fabricated an FOMI probe using a femtosecond laser for temperature sensing purposes.<sup>[70]</sup> The probe showed a linear response and a sensitivity of  $4.28 \text{ nm } ^\circ\text{C}^{-1}$ . The probe was found to have a great potential for application in harsh environments. Furthermore, FOMI has been developed for low-frequency

acoustic sensing/noise pollution monitoring based on a gold diaphragm.<sup>[71]</sup> Recently, the FOMI probe was reported for seismic monitoring.<sup>[72]</sup> The measurements were carried out under simplified conditions using a calibrated stroke as a standard loading. The measured value of the amplitude and oscillation velocity matched with those measured by commercial seismic devices with an average deviation of 0.02. The applications of the FOMI extended to detect the magnetic fields. For instance, an in-line FOMI probe was developed based on single-mode fiber and hollow-core fiber.<sup>[73]</sup> The magnetic field of the magnetic fluid was influenced by the applied magnetic field changing the effective refractive index of the cladding leading to shifting the reflected spectrum. The probe showed a sensitivity of  $118.7 \text{ pm mT}^{-1}$  for the magnetic field in the range of 1.36–11.8 mT. The FOMI probe was found to have the potential for detecting weak magnetic fields.

Processing the output signals, the necessity for bulky instruments, and coherent light sources are considered the drawbacks of the FOMI probes. In contrast, FOMI probes showed to have all advantages of the FOMZI probes, in addition to the significant advantage of pluggable measurements, which can be considered as an excellent foundation for the application of such sensors in *in vivo* measurements.

#### 5.4. Fiber-Optic Sagnac Interferometer (FOSI)

FOSI is composed of three-terminal couplers, two polarization controllers, and an optical fiber loop along with two light beams of different polarization states propagating in counter directions (Figure 2i). The launched light beam is split by the coupler into two counter-propagating beams, which recombine at the same coupler. A birefringent fiber is utilized in the sensing section of the loop to maximize the polarization dependence of the FOSI. The phase of the interference is obtained by

$$\delta_{SI} = (2\pi/\lambda)BL, \quad B = |n_f - n_s| \quad (9)$$

where  $B$  refers to the birefringent coefficient of the sensing fiber,  $L$  denotes the length of the sensing fiber, and  $n_s$  and  $n_f$  represent the effective refractive index of the slow and fast modes.<sup>[74]</sup>

FOSI sensors have been employed in sensing temperature, strain, salinity, hydrogen, ultrasonic waves, and pressure.<sup>[74,75]</sup> For instance, a highly sensitive temperature sensor was developed based on fiber Sagnac interferometer combined with photonic crystal fiber (PCF).<sup>[76]</sup> Two side holes of the PCF were filed with metals which allowed for changing the birefringent of the fiber due to expansion of the used bismuth and indium. A sensitivity of  $9 \text{ nm } ^\circ\text{C}^{-1}$  was achieved by using indium-filled side-hole PCF. The high sensitivity is attributed to the fiber microstructure which modulated the birefringence of the PCF by expanding the metal-filled holes. FOSI was found to be more sensitive to temperature than both LPFG and FBGs. A study showed that FOSI provided a sensitivity of one- to two-orders magnitude higher than that of the temperature sensitivity for LPFG and FBGs, respectively.<sup>[75c]</sup> Fu et al. proposed a pressure sensor that was realized by polarization-maintain photonic crystal fiber (PM-PCF)-based Sagnac interferometer.<sup>[77]</sup> A sensitivity of  $3.42 \text{ nm MPa}^{-1}$  was detected for the sensor. The pressure sensor was relatively low-temperature-sensitive due to the low thermal

dependence and bending loss of the used PM-PCF. Also, FOSI probes have been developed recently for detection the cancer affected cells based on the cells' refractive index which is different than those of the normal cells.<sup>[78]</sup> The probe showed to be sensitive for Jurkat, PC1, MCF-7, and MDA-MB-231 cells.

The sensitivities of the traditional optical fiber sensors are very limited due to the light confinement in the fiber core, so the interaction between light and analyte is very weak. The FOSI can overcome these shortcomings – offering strong light–analyte interaction and consequently, high sensitivity. In addition to it is high sensitivity, FOSI probes have simple structures and are easy to fabricate. Therefore, FOSI probes have attracted attention in various sensing applications. However, the birefringent fiber used for sensing in the FOSI probe is highly sensitive to temperature. Furthermore, FOSI probes have relatively large volumes due to the need to take the ring shape, which makes it unpractical for insertion or implanting sensing.<sup>[74]</sup>

## 6. Surface Plasmon Resonance-Based Fiber-Optic Sensors (SPR)

Surface plasmon resonance (SPR) can be subdivided into planer and localized surface plasmons. The planer surface plasmon phenomenon was discovered in 1902 through observing anomalies in the spectrum of the light reflected from a metal diffraction grating.<sup>[79]</sup> Fano proved that these anomalies were due to the excitation of electromagnetic surface waves on the surface of the diffraction grating.<sup>[80]</sup> Otto demonstrated that bringing a prism close to a metal–dielectric interface can excite surface plasmons. Kretschman and Raether built an optical setup to demonstrate the excitation of surface plasmons, which is considered the basis of the current research and commercial surface plasmon resonance instrumentations. The setup involved a quartz  $60^\circ$  prism of a base coated with a silver film of thickness of 50 nm (Figure 3a). The excited surface plasmons were maximum at the silver film–air interface and followed an exponential decay trend in both silver and air media. Transverse magnetic (TM) polarized waves are required to excite surface plasmons because the surface plasmons are TM waves in nature. The propagation constant of surface plasmons according to the solution of Maxwell's equations for the metal–dielectric interface is

$$K_{sp} = K_o(\epsilon_s \times \epsilon_m / \epsilon_s + \epsilon_m)1/2 \quad (10)$$

where  $K_{sp}$  denotes the propagation constant of the surface plasmons,  $K_o$  is the free-space propagation constant of the incident light, and  $\epsilon_s$  and  $\epsilon_m$  are the dielectric constants of the dielectric and metallic layers.<sup>[84]</sup> The propagation constant of the surface plasmons is higher than that of the incident light. Therefore, direct incident light solely is not enough to excite surface plasmons. Thus, additional energy or momentum along with the energy of the incident light is essential to excite surface plasmons. Coupling the incident light using a prism, grating, waveguide, or optical fiber can excite surface plasmons.<sup>[85]</sup>

In contrast, light interaction with nanoparticles induces collective oscillations of the metal's free electrons in the conduction band, which is defined as localized surface plasmon (LSP) (Figure 3b). Unlike the planar surface plasmon resonance in

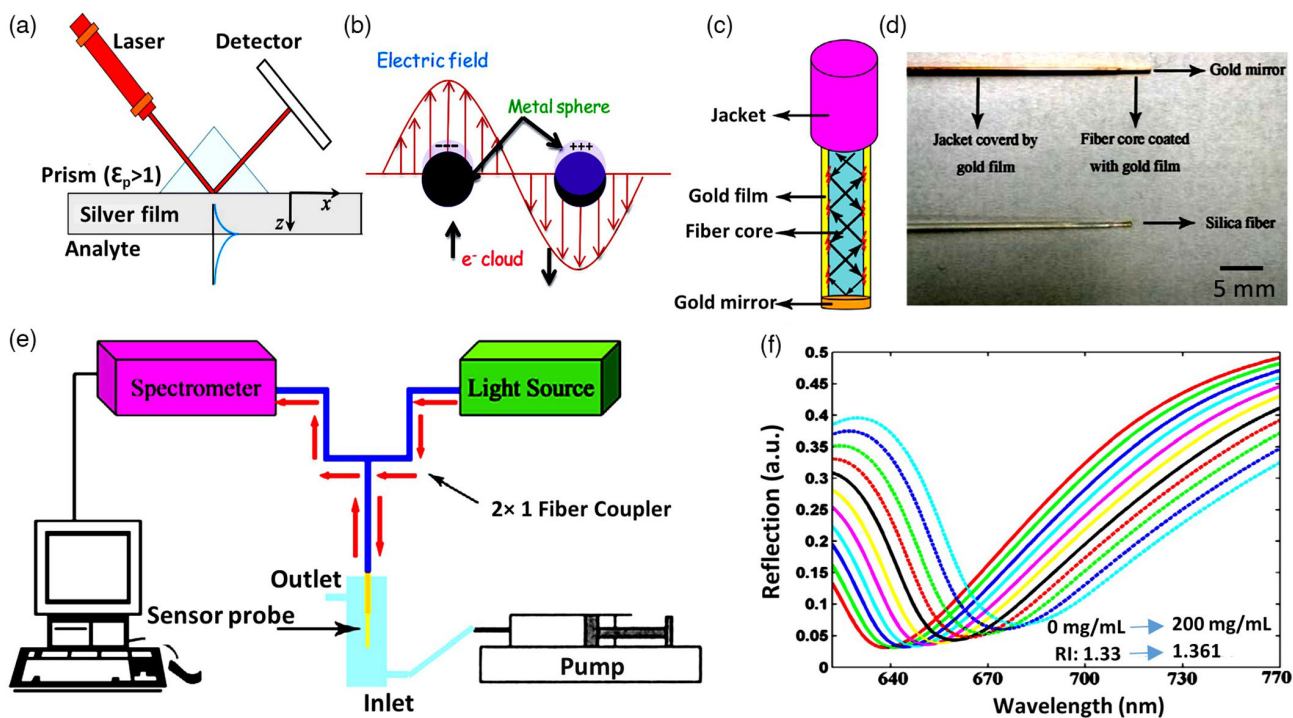


**Figure 3.** Surface plasmon resonance (SPR) phenomenon and its implementation in fiber-optic for sensing. a) The setup made by Kretschmann for exciting planar surface plasmon resonance, the blue curve represents the profile of the excited field. Reproduced with permission.<sup>[81]</sup> Copyright 2018, The American Physical Society. b) Light interaction with a metal nanoparticle inducing localized surface plasmon resonance. Reproduced with permission.<sup>[82]</sup> Copyright 2016, The Royal Society of Chemistry. c) SPR-based fiber probe. d) A photograph of the SPR fiber optic probe. e) The setup for testing the SPR-based fiber probe. f) Transmission spectra of the SPR-fiber probe exposed to various glucose concentrations having different refractive indices. (c–f) Reproduced with permission.<sup>[83]</sup> Copyright 2015, Institute of Physics Publishing, Ltd.

which the surface plasmon waves are confined at the metal–dielectric interface, the LSP is localized on the surface of the metal nanoparticles.<sup>[85]</sup> The interaction of the electric field of the incident light with the free electrons of the metal nanoparticles separates the electrons from the positive ions (nuclei). The Coulomb attraction force between the ions and the free electrons leads to recombination. Therefore, the collective oscillations of the free electrons induce excitation of localized surface plasmons (Figure 3b).<sup>[86]</sup> Excitation of LSP resonance (LSPR) is marked by an enhancement in the absorption of the incident light at the surface of the metal nanoparticles. The LSPR phenomenon depends on the size, type, and shape of the nanoparticles, the wavelength of the incident light, and the refractive index of the surrounding dielectric medium.<sup>[87]</sup> In LSPR, the absorbed wavelength of the incident light changes based on the refractive index of the surrounding medium of the nanoparticles. Thus, changing the refractive index of the particles medium is transformed into a shift in the resonance absorption, which appears in the measured transmission and absorption spectra. The latter is the working principle of LSPR sensors.<sup>[88]</sup> The correlation of the absorbed/resonant wavelength and the refractive index of the medium surrounding the nanoparticles is given by

$$\Delta\lambda = S(\Delta n)[1 - \exp(-2d_m/L_d)] \quad (11)$$

where  $\Delta\lambda$  is the wavelength shift in the absorption spectrum corresponding to the change in the refractive index of the

nanoparticles' medium ( $\Delta n$ ),  $S$  is the refractive index sensitivity,  $d_m$  refers to the thickness of the surrounding medium of the nanoparticles, and  $L_d$  denotes to the decay length of the associated electromagnetic field.<sup>[89]</sup>

Surface plasmons are excited in optical fibers through the total internal reflection. When a polychromatic light beam is launched in an optical fiber, the guided modes propagate in the fiber's core and the evanescent waves propagate in the fiber cladding. The guided modes are subjected to total internal reflection at the core–cladding interface and they exponentially decay into the fiber cladding. In the optical fiber, the core-guided waves are the incident light rays on the core–cladding interface with angles in the range of  $\theta_c$ – $90^\circ$ , where  $\theta_c$  is the critical angle of the fiber core–cladding interface. For inducing surface plasmons in the optical fiber, a small section of the fiber cladding is removed and replaced with a thin plasmonic film, usually silver or gold of 50 nm thickness. Matching the wave vector of the evanescent waves propagating at the fiber core–metal interface with that of the surface plasmon waves propagating at the metal–dielectric interface induces the SPR which is marked by a dip in the transmitted spectrum. The light absorbed band which appears in the transmission spectrum is wider than that originated by other coupling techniques such as gratings and prisms. Because the guided waves in the fiber have a range of total internal reflection angles, and at each angle, an SPR is induced resulting in a broad SPR band that influences the sensing parameters of the fiber

probe such as the limit of detection and the sensitivity. Among the coupling components, the excitation of surface plasmon waves by optical fibers presents a compact and efficient method that has advantages compared to prisms and gratings.

To fabricate a plasmonic fiber probe, the fiber cladding of a small section is peeled off, followed by coating the fiber core with a thin layer of a plasmonic material. The analyte to be tested is introduced into the plasmonic section of the fiber. Upon launching the polychromatic light into the fiber, evanescent waves originate at the fiber core–metal interface, inducing surface plasmons at the metal–analyte interface. Consequently, a sharp dip in the transmission spectrum of the fiber is recorded confirming the resonance absorption at specified wavelengths called the resonance wavelengths. Modulation in the refractive index of the analyte medium results in a shift in the resonance wavelengths, and this is the sensing mechanism of the fiber probes based on SPR. The chosen plasmonic material for exciting surface plasmons has a significant role in the flexibility of the fabrication process and performance of the SPR-based fiber probes.<sup>[85]</sup> Silver and gold are preferable plasmonic metals due to their superior optical properties in the visible and near-infrared ranges. Silver presents unparalleled plasmonic characteristics in the visible region due to its low dielectric loss; however, it suffers from poor chemical stability.<sup>[90]</sup> Gold is the most common metal used in SPR applications because of its high chemical stability. SPR-based fiber has been used for a wide range of sensing applications; however, the limited penetration depth of the evanescent waves into the analyte medium is a

challenge posing restrictions on sensing large molecules such as proteins.<sup>[91]</sup> For instance, a straight fiber-optic probe for non-selective glucose detection was reported.<sup>[83]</sup> A small segment of the fiber was coated with a gold layer and the fiber tip was coated with a gold mirror as well (Figure 3c,d). The reflection spectrum from the probe shifted to longer wavelengths when the glucose concentration in the tested solution increased. The glucose concentration was correlated to the resonance wavelength by the relationship:  $\lambda_{\text{res}} = 634.3 + 0.13 M + 0.001 M$ , where  $\lambda_{\text{res}}$  denotes the resonance wavelength and  $M$  refers to the glucose concentration in  $\text{mg mL}^{-1}$ . The setup used to interrogate the fiber probe, and the measured transmission spectra at various glucose concentrations, are shown in Figure 3e,f. To increase the leakage of the fiber-guided light into the cladding region for the purpose of enhancing the sensitivity of the probe, and unconventional optical fiber probe was developed which comprised two different core diameter fibers: 50 and  $3 \mu\text{m}$ <sup>[92]</sup> (Figure 4a). The silver film was uniformly sputtered on the cladding surface for exciting SPR. The probe demonstrated a response for the refractive index changes from 1.333 to 1.398 for which the resonant wavelength red-shifted from 527 to 735 nm (Figure 4b). A similar fiber probe was introduced for pH sensing by coating a pH-responsive hydrogel on the fiber cladding covered with a silver film.<sup>[93]</sup> The interaction of  $\text{H}^+$  ions in pH solutions with the pH-responsive hydrogel induced volumetric and refractive index changes which led to shifting the SPR wavelengths. A similar fiber probe was developed for glucose sensing in aqueous solutions.<sup>[94]</sup> The probe was fabricated by

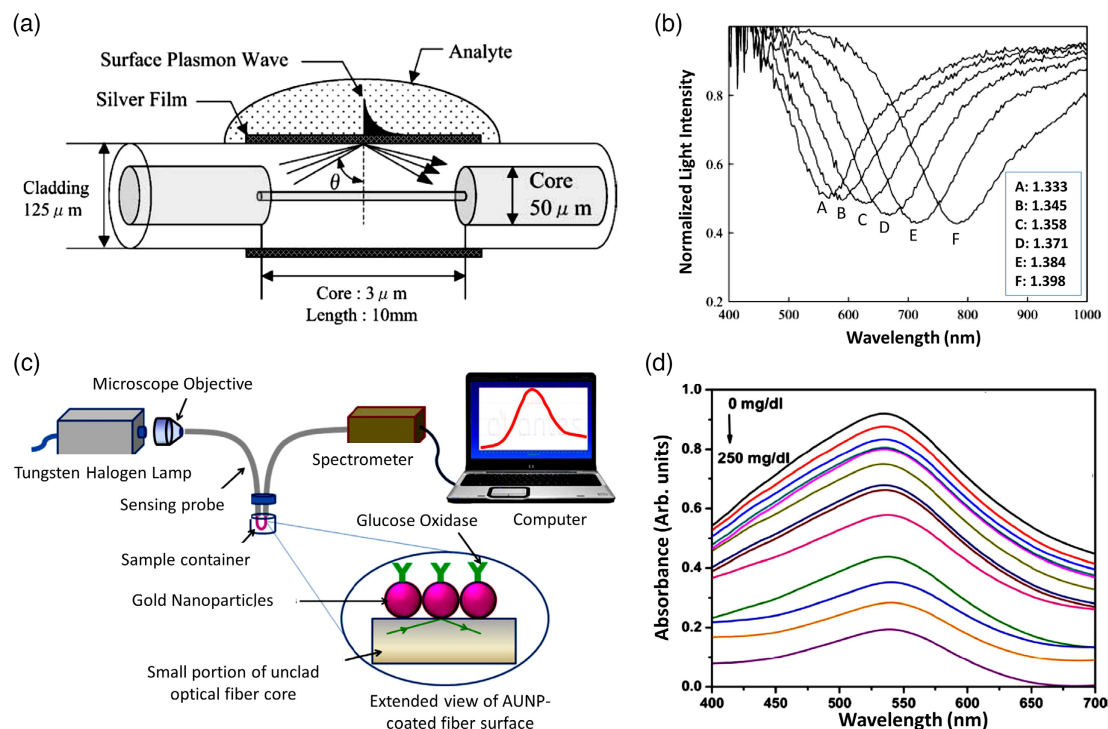


**Figure 4.** SPR-based fiber sensors: a) A hetero-core structure fiber probe with a silver layer deposited on the cladding of a single-mode fiber, b) transmission spectra of the plasmonic probe while the silver coating exposed to media of different refractive index. (a and b) Reproduced with permission.<sup>[92]</sup> Copyright 2004, Elsevier. c) The interrogation setup used to test the U-shape LSPR resonance (LSPR) fiber sensor, and d) absorption spectra of the U-shape fiber probe in the glucose concentration range of 0–250  $\text{mg dL}^{-1}$ . (c and d) Reproduced with permission.<sup>[96]</sup> Copyright 2011, Springer Nature.

coating a small section of the optical fiber's core with a silver layer, then a silicon film followed by a hydrogel film trapping glucose oxidase. The silicon film was deposited on the silver layer to enhance the sensitivity. A 20 nm blue shift in the resonance wavelength was detected with glucose concentration in the range of 0–260 mg dL<sup>-1</sup>. The fabrication process of the probe is summarized to highlight the required instruments and the level of complexity. A multimode fiber of a core thickness 600 μm and numerical aperture 0.4 was used. A tungsten cutter was used to sharpen the fiber ends for improving the light coupling and a blade was utilized to peel off the cladding of the fiber segment. The uncladded region was cleaned by nitric acid, rinsed with deionized water and acetone for 4–5 times, followed by ion doping in a vacuum chamber. A silver film of 40 nm thickness was deposited on the cleaned uncladded section followed by a 7 nm thick silicon layer. Both layers, silver and silicon were prepared by the thermal evaporation technique at room temperature under a pressure of  $5 \times 10^{-6}$  Torr. Glucose oxidase was immobilized in a gel, and the probe was dipped into it to be coated with the glucose-responsive layer. The readout procedure included: 1) an unpolarized light source was coupled with the fiber at one end with a microscope objective lens; and 2) the transmitted light through the fiber was collected from the other end by a spectrometer which was connected to a computer. The transmitted spectra were processed, and the resonance wavelength was detected at various glucose concentrations. For methanol detection, a plasmonic fiber probe was reported based on a nanohole gold film along with an epoxy layer.<sup>[95]</sup> A MoS<sub>2</sub> layer was used to improve the sensitivity of the sensor. The probe was found insensitive for relative humidity in the range of 11–92%RH and stayed stable for a year, which demonstrated its high potential for practical applications.

For applications in food and water quality monitoring, Siddharth et al. developed an SPR-based probe for detecting *Escherichia coli* (E.coli).<sup>[97]</sup> Recently, a plasmonic fiber probe was developed for breast cancer detection.<sup>[98]</sup> The probe relied on a silica fiber coated with a gold layer and loaded with HER<sub>2</sub> antibodies. The cancer biomarker concentration as low as 10 ng mL<sup>-1</sup> (≈86 pM) was detected. Not only glass/silica fibers were used for inducing SPR and for sensing applications but also plastic fibers have been used. For instance, straight plastic optical fiber was coated with gold/palladium alloy and functionalized with anti-cortisol antibody, and passivated with bovine serum albumin for cortisol sensing application.<sup>[99]</sup> The probe was tested in different cortisol concentrations in the range of 0.005–10 ng mL<sup>-1</sup>. The resonant wavelength of the tested probe shifted 15 nm for the tested concentration range and the limit of detection was 1 pg mL<sup>-1</sup>. The probe showed a sensitivity of 15-fold higher than when it was functionalized with anti-hCG antibodies that showed 1 nm shift in the same cortisol concentration range.

As the penetration of the evanescent waves and the interaction with the dielectric analyte medium are the basis of the SPR-based fiber sensors, it is essential to adequately expose the evanescent waves to the analyte medium. To increase the evanescent waves that reach the analyte medium, numerous geometries of the optical fiber probes have been proposed including D-tube, tapered, and U-bent.<sup>[96,100]</sup> For example, a U-shape fiber probe was developed for glucose detection (Figure 4c).<sup>[96]</sup> The probe included gold nanoparticles attached to the fiber core, and the glucose

oxidase was immobilized over. Oxidizing the glucose oxidase in the presence of glucose solution led to a change in the refractive index of the film inducing a change in the absorption intensity of the resonant wavelengths of the gold nanoparticles (Figure 4d). Bending the fiber probe had a significant influence on the probe's sensitivity, and the bending radius of 0.982 mm achieved the maximum sensitivity. The required blood sample was 150 μL which is less than the amount demanded commercial sensors (1.5 mL). Selective glucose probes do not only rely on enzymes such as glucose oxidase and glucose peroxidase but also on phenylboronic derivatives, which were introduced for long-term glucose monitoring. For instance, a self-assembled of *p*-mercaptophenyl boronic acid (PMBA) was deposited on a gold-coated fiber.<sup>[101]</sup> Interaction of *cis*-diol molecules such as glucose with the PMBA monolayer deposited on the gold layer induced a change in the monolayer's refractive index. The response of the probe for glucose variation was insignificant because of the low molecular mass of glucose, consequently, no shift in the excited SPR wavelength was recorded. Therefore, gold nanoparticles modified with 2-aminoethanethiol (AET) and PMBA were introduced to enhance the sensing performance of the probe. The resonance wavelengths of the probe were red-shifted with glucose concentration variation and demonstrated a significant response to glucose concentration in the range of 0.01–30 mM. The probe was highly sensitive for glucose concentration presenting a limit of detection of 80 nM. However, the performance of the probe was limited by both the long response time (12 min) and the saturation time (53 min). Xie et al. developed a plasmonic fiber probe which had a U-shape design and was coated with graphene for refractive index sensitivity.<sup>[102]</sup> The combination of graphene and U-shape design improved the sensitivity of about fivefold as compared to the conventional gold-based straight plasmonic fiber. The refractive index sensitivity of 15.52 μm RIU<sup>-1</sup> was achieved by depositing a monolayer of graphene over the gold layer on the U-shaped fiber of a bent radius of 1.1 cm. Manoharan et al. developed a U-bent shape plasmonic fiber probe made of glass and polymer.<sup>[103]</sup> Ni/NiO was deposited on the U-region using the sputtering technique prior to growing the gold nanostructures. The sensitivity for the refractive index for polymer and glass fiber probes were 27.66 and 25.65 ΔA/ΔRIU, with plasmonic peaks at 600 and 570 nm, respectively. Divagar et al. developed a plasmonic fiber probe for tuberculosis (TB) diagnosis.<sup>[104]</sup> The fiber probe was U-bent and loaded with gold nanoparticles functionalized with anti-M<sub>tb</sub> LAM immunoglobulin M (IgG). M<sub>tb</sub> LAM which is a TB biomarker and present in urine, was quantified by detecting the change in light absorption passing through the fiber probe connected with a green LED and a photodetector. A plasmonic plastic fiber was reported for the detection of chikungunya viral disease.<sup>[105]</sup> The non-structural protein 3 (CHIKV-nsP<sub>3</sub>) was used as the biomarker. The plastic fiber with core diameter of 0.5 mm was designed in U-shape and gold nanoparticles were used as labels. Light absorption by the gold nanoparticles changed upon formation of a sandwich immunocomplex of CHIKV-nsP<sub>3</sub>. The probe showed a linear response in the range of 1–104 ng mL<sup>-1</sup> and limit of detection of 0.52 ng mL<sup>-1</sup>. Additionally, the probe showed specific sensitivity toward the CHIKV-nsP<sub>3</sub> than for Pf-HRP<sub>2</sub>, HIgG, and dengue whole virus.

Optical fiber-based SPR sensors have replaced the traditional substrate-based SPR sensors, due to their ability to analyze minute samples, providing remote sensing and compact design. Currently, the SPR-based fiber sensors are used for numerous applications, including biomedical diagnostics, environmental safety, and life science. However, the signal-to-noise ratio limits their functioning window, sensitivity, and resolution.<sup>[106]</sup> Furthermore, the propagating modes in multimode fibers are nearly random and the mode distribution at different incident angles is unsteady. Also, the SPR-based multimode fiber sensors are sensitive to mechanical disturbance which influences the quality of the output signal. In contrast, an SPR probe based on single-mode fiber shows a narrow resonance dip in the transmission spectrum, which results in an enhanced limit of detection. Hence, the single-mode fiber is preferable. For enhancing the sensitivity and resolution of the SPR-based probes, thin films of graphene, molybdenum disulfide, molybdenum diselenide, tungsten disulfide, and tungsten diselenide, are added to the plasmonic metal layer.<sup>[107]</sup> However, challenges such as the multistage and sophisticated fabrication process, and the need for costly equipment are still open.<sup>[101]</sup>

## 7. Fluorescence-Based Fiber-Optic Probes (FF)

Fluorescence denotes the light emission from a substance shortly after absorbing light of higher energy. This phenomenon occurs when an incident light in the wavelength range of 200–800 nm is absorbed by fluorescent molecules – raising certain electrons to higher energy levels.<sup>[108]</sup> Then, the excited molecule loses some of the absorbed energy by emitting light returning to the ground state. Some of the absorbed light is lost in form of heat or vibration, consequently, the emitted light has lower energy than that of the absorbed. The electronic transition from an energy level to a higher level due to light absorption is an instantaneous process ( $10^{-15}$  s), and the lifetime of the excited state is around  $10^{-8}$  s. Accordingly, the whole process of fluorescence emission lasts about  $10^{-8}$  s.<sup>[109]</sup> The excited fluorescent molecules (fluorophores) can lose the absorbed light not only by re-emission, heat, or vibration, but also by transferring the energy to another fluorophore nearby. If a portion of the exiting energy is transferred from a donor fluorophore to a ground state of an acceptor fluorophore, the process is called Förster resonance energy transfer (FRET).<sup>[110]</sup> The portion of the transferred energy depends on the spectral overlapping between fluorophores and the interspace between them.<sup>[111]</sup> Förster resonance energy transfer is considered a suppression process for the absorbed energy by a donor fluorophore as the energy drains to a nearby acceptor fluorophore.

A fluorescence-based sensor can be constructed of a certain analyte-receptor/molecular recognition agent, a donor fluorophore, and an acceptor fluorophore; all of these constituents must lie in the vicinity of each other. Once the analyte binds with the receptor, the receptor undergoes a chemical structural change – moving the fluorophores farther apart to limit transferring electrons to the acceptor fluorophore. Consequently, the FRET decreases, resulting in an increase in the fluorescent emitted light which is correlated to the analyte concentration (Figure 5a). A receptor/molecular recognition agent can be used in fluorescent sensors to competitively bind with an analyte.<sup>[112]</sup>

In this mechanism, the fluorophore is bound to the receptor, and the electrons transfer from the fluorophore to the receptor. However, the existence of the analyte induces the separation of the fluorophore from the receptor. In this method, the higher the analyte concentration, the lower the fluorescence emission.<sup>[113]</sup>

Progress in polymeric materials has led to enhancing the optical performance of the hydrogel optical fibers.<sup>[116]</sup> Fluorescent hydrogel fibers were developed for implantable in vivo sensing. For example, a hydrogel fiber was made of a biocompatible material (polyethylene glycol-polyacrylamide) for glucose detection (Figure 5b).<sup>[115]</sup> The fiber was functionalized with glucose-responsive fluorescent microbeads and was inserted underneath the skin. Images of the fluorescent fiber were taken by a camera and processed to measure the fluorescence intensity at various glucose concentrations. The fluorescent intensity at the wavelength 488 nm increased with glucose concentration in the range from 0 to 500 mg dL<sup>-1</sup>.<sup>[115]</sup> The glucose-responsive fluorescent microbeads were prepared by an axisymmetric flow-focusing microfluidic device (AFFD), which produced a mono-disperse droplet of the glucose-responsive pre-gel. The droplets were polymerized and washed to remove the unreacted ingredients.<sup>[117]</sup> The fluorescent microbeads were mixed with the optical fiber pre-gel (acrylamide and polyethylene glycol diacrylate) and injected into an optical fiber mold. The gel was stored for 30 min at a temperature of 37 °C to polymerize.<sup>[115]</sup> Also, fluorescent probes were developed by attaching the fluorescent sensors to the fiber tip. For example, a fluorescent hydrogel sensor was attached to the distal end of a silica multimode fiber with a diameter of 125 μm.<sup>[118]</sup> A calcium-fluorescent indicator was crosslinked with acrylamide through vinyl groups during the free-radical polymerization process. The fluorescent light recorded at the opposite end of the probe increased with calcium concentrations. The cancerous lung tissues were recognized by a fluorescent fiber probe made of a multimode fiber having a tip functionalized with a pH-sensitive fluorescent hydrogel.<sup>[119]</sup> The developed fiber probe showed a linear response in the physiologically relevant pH range of 5.5–8.0 with a precision of 0.10 pH units. Also, the acidity of the cementitious materials was detected by a fluorescent fiber probe based on a pH-dependent fluorescent dye.<sup>[120]</sup> The pH-fluorescent responsive dye (Naphth-AlkyneOMe) was cross-linked in polyvinyl alcohol glutaraldehyde matrix to generate a thin film with an average thickness of 150 μm deposited on the tip of the fiber. The probe was tested on the surface of low-pH cement paste after 4, 6, 7, and 8 days of hydration. The probe showed a reversible response to pH changes and the response time was 100 s. Furthermore, fluorescent fiber probes were recently reported for antibiotic detection, ciprofloxacin (CIP).<sup>[121]</sup> The fluorescent sensor combining nanoparticles composite of polyethylene glycol diacrylate hydrogel and antibiotic detective agent was attached to the optical fiber tip and tested for ciprofloxacin detection in aqueous solutions. A linear relationship between the concentration of the CIP and the fluorescent intensity with a correlation coefficient 0.99 was obtained and the limit of detection (LOD) reached to 6.86 μM. For environmental applications, fluorescent fiber probes have been developed for toxic heavy metal ions. For instance, Liu et al. developed a fluorescent probe for Cd<sup>2+</sup> detection in aqueous solutions.<sup>[122]</sup> The effective detection range of the probe

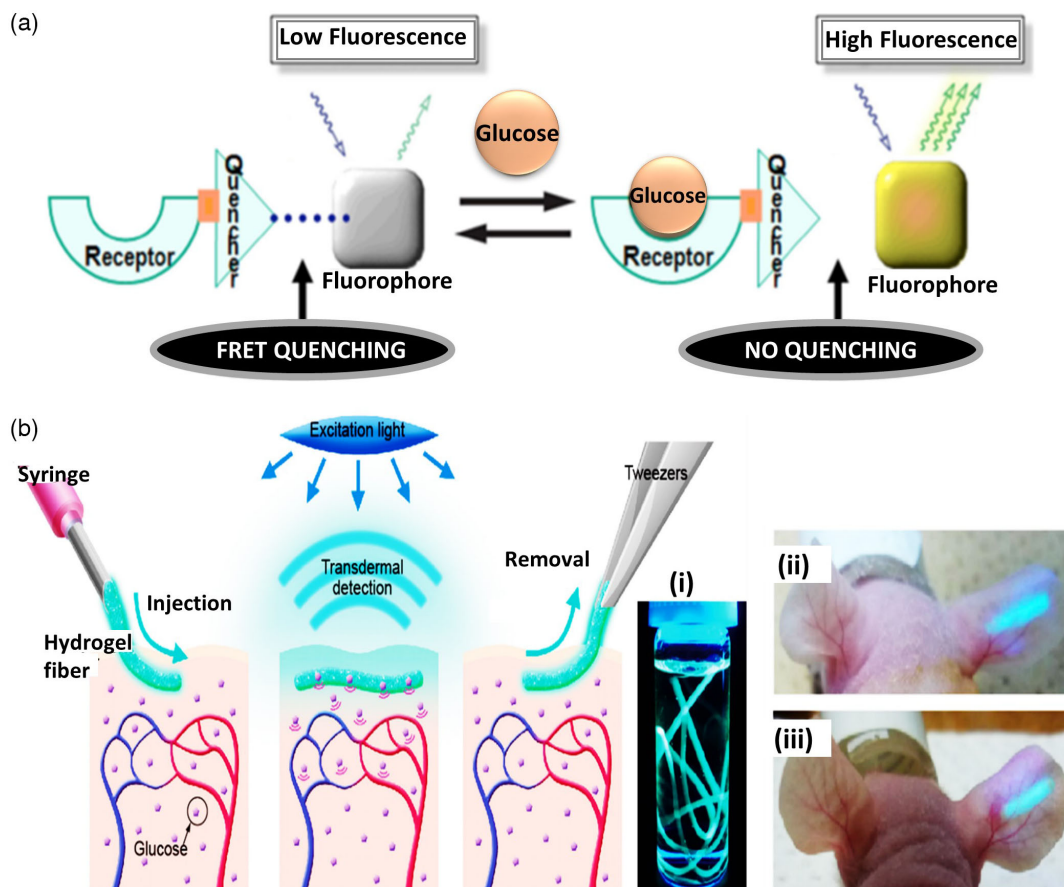


**Figure 5.** Fluorescent fiber-optic probes. a) Working principle of a fluorescent glucose sensor based on Förster energy transfer. Reproduced with permission.<sup>[114]</sup> Copyright 2012, SAGE Publications. b) The fluorescent fiber probe injection, working principle, and removal process: i) The fluorescent hydrogel fiber probe in a glass vial soaked in a 50 wt% glucose solution, ii–iii) Photos of the fluorescent fiber probe immediately after insertion in a mouse ear and after 30 days, respectively. Reproduced with permission.<sup>[115]</sup> Copyright 2011, PNAS.

was in range of 0.1–290  $\mu\text{m}$ , with a limit of detection of 37.8 nM. The probe was proved to be capable of detecting  $\text{Cd}^{+2}$  in lake water samples and meets the WHO standard. Copper ions have been recently detected by a fluorescent fiber probe based on AGInZnS quantum dots (QDs) fabricated in polyvinyl alcohol matrix which was deposited on the tip of the optical fiber.<sup>[123]</sup> The fluorescence of the QDs was quenched by Cu(II) resulting from both static and electron transfer from QDs to Cu (II). The probe was selective and showed a linear detection range of 2.5–800 nM. Recently, iron ion ( $\text{Fe}^{3+}$ ) was detected using  $\text{Eu}(\text{BPDA})_{1.5}\text{phen}@\text{PAN}$  fluorescent fiber prepared by electrospinning of the polyacrylonitrile (PAN).<sup>[124]</sup> The fluorescence quenching was observed by naked eye upon exciting the fiber with ultraviolet light. The developed fiber showed high sensitivity and low limit of detection (0.063), providing a promising strategy for developing flexible sensors for  $\text{Fe}^{3+}$  monitoring.

Fluorescent fiber-optic sensors are very sensitive and offer a low limit of detection. However, their applications are limited due to the photobleaching of the fluorophores. When the fluorophores get exposed to the light of a specific wavelength, they transit from the ground state to the excited state and the total number of the transition cycles between excitation and emission of each

fluorophore molecule depends on its chemical structure and the local environment. Based on these parameters, some fluorophores bleach quickly, while others undergo several cycles of excitation and emission before bleaching. However, reducing the intensity of the excitation light may reduce the photobleaching. Also, decreasing the time of light exposure may assist in reducing the photobleaching effect. However relying on the fluorescence intensity changes in response to the analyte is the most simple and direct method, fluctuation of the illuminating light source is a concern, which leads to under/overestimation of the analyte concentration.<sup>[125]</sup> It is unreliable and inconvenient to use intensity changes, which may occur for a variety of reasons. It is more practical to use wavelength-ratiometric fluorescent probes which show a shift in the emission/absorption spectra upon binding with the analyte. These fluorescent probes are favorable because the ratios are independent of the light source fluctuation. In this case, the analyte concentration is determined from the ratio of the fluorescent intensities measured at two excitation or emission wavelengths. Another ratiometric method that can be used in sensing, is fluorescence polarization or anisotropy. In this method, the analyte induces a change in the anisotropy of the label and the anisotropy values

are calculated using the ratio of the polarized intensity measurements, which makes the anisotropy independent of fluctuation of the light sources and fluorophore concentration as long as the measurements are not distorted by autofluorescence or poor signal-to-noise. Also, fluorescence lifetimes can be used for sensing and the lifetime can be measured using either frequency-domain or time-domain methods. A few years ago, this method has been considered too complex for sensing applications; however, the recent advances in electro-optics technology made it feasible to perform nanosecond decay time measurements. It is expected that the use of lifetimes for sensing would revolutionize the fluorescent sensors by making them capable of providing the long-term stability which is needed for real-world applications.

## 8. Light Diffuser-Integrated Optical Fiber Sensors (LDOF)

Recently, optical fiber probes based on light diffusers were developed for metabolites monitoring.<sup>[126]</sup> The probes are based on stimuli-responsive hydrogels which are imprinted with light-diffusing microstructures (LDMs) and chemically attached to the distal ends of traditional optical fibers. The LDMs can be considered as a dense-packed microparticle on a substrate (Figure 6a). The dense-packed particles have various geometries and dimensions. They scatter the incident light beam in the forward and backward directions at different angles to project a diffused spot of the light on screens fixed in transmission or reflection

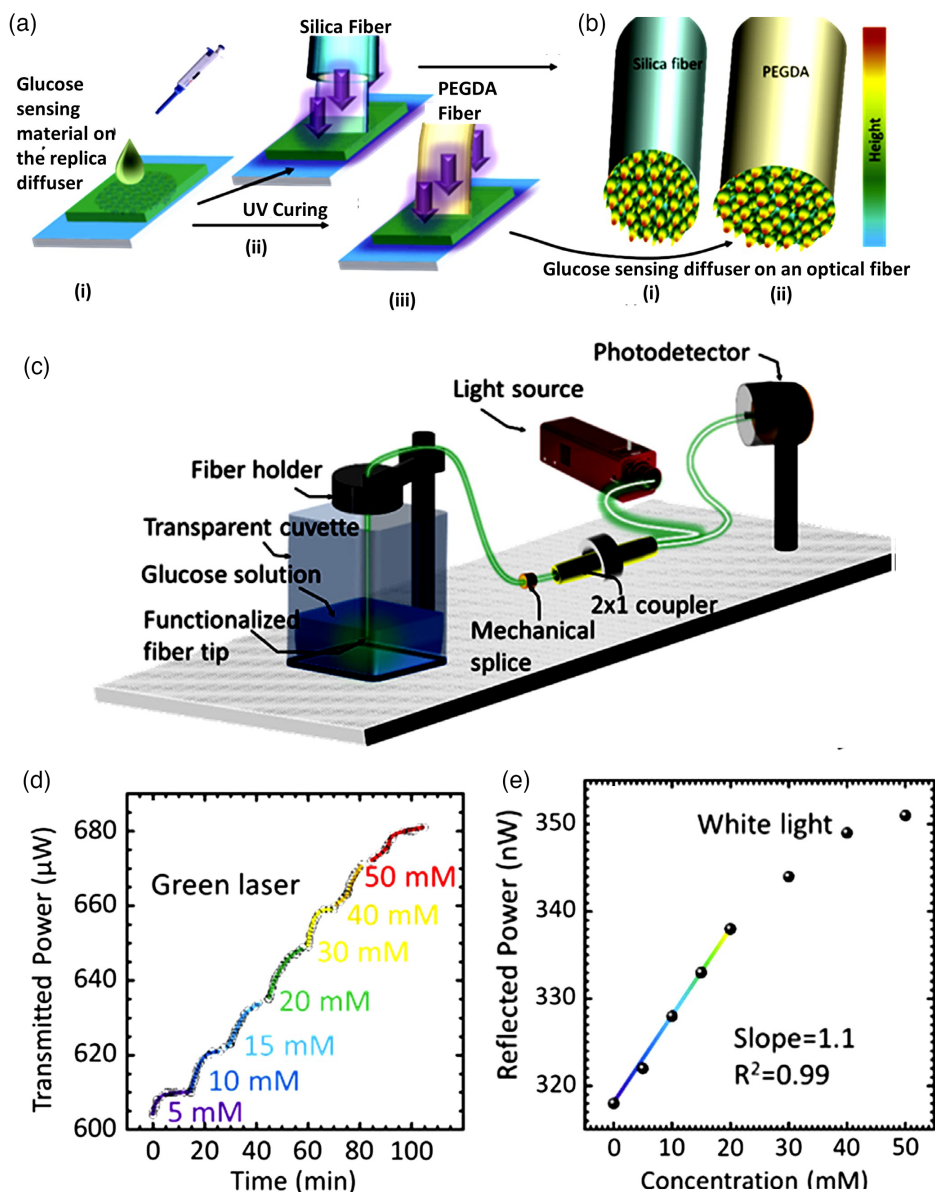


**Figure 6.** Light diffuser-based fiber optic sensor: a) Sensor fabrication process, b) fabricated probe, c) interrogation setup for testing the performance of the fiber probe, d) transmitted optical power of the fiber probe versus time while the probe was immersed in various glucose concentrations, e) The measured reflected power versus glucose concentrations. Reproduced with permission.<sup>[126b]</sup> Copyright 2019, Elsevier.



configurations. If the LDMs were made of analyte-responsive hydrogels and attached to a tip of an optical fiber, the LDMs hydrogel undergoes a volumetric shift upon interaction with the targeted analyte. The volumetric modulation induces a change in the refractive index and dimensions of the LDMs – resulting in modification of the scattering efficiency of the LDMs; subsequently, angles of scattered light in the forward and backward directions are altered. Three fiber probes were developed for monitoring glucose, pH, and alcohols (Figure 6b). The glucose-responsive hydrogel was made of a polyacrylamide hydrogel matrix and 3-(acrylamido)phenylboronic acid which functions as a glucose recognition agent.<sup>[126b]</sup> The probe performed under the physiological conditions and showed a high sensitivity ( $2.6 \mu\text{W mL}^{-1}$ ), rapid response (30 s), and saturation time (15 min). The probe was tested in the reflection configuration to confirm its practicality, and an optical power meter was used as a reader. However, in the transmission configuration, a smartphone was used as a compatible readout device (Figure 6c–e). The alcohol and pH probes were based on poly(HEMA) and showed a robust performance.<sup>[126a]</sup> The alcohol probe instantaneously responded to propan-2-ol, ethanol, and sulfoxide dimethyl. The pH probe showed a rapid response and high sensitivity to pH changes in the acidic region. The pH probe recorded sensitivities of 40 and 7 nW  $\text{pH}^{-1}$  in transmission and reflection configurations, respectively.

This class of fiber probes overcomes some limitations such as the need for bulky instruments for the output data processing. Also, the readout methodology is simple and practical, and the fabrication process can be carried out in a single step. However, this probe relies on measuring the optical power which is influenced by the fluctuation of the light source illumination.

## 9. Comparison among the Optical Fiber Sensors' Approaches

Optical fibers as a light transducer have been explored for their potential as sensing devices in the past decades. Numerous achievements have been realized in optical fiber sensing applications due to the great demand for small-size sensors, remote, and real-time monitoring. Now, optical fiber sensors have been developed for diagnostic, drug delivery, environmental monitoring, explosive gas detection, etc. Compared to other kinds of sensors, optical fiber sensors provide versatility of multiplex detection and remote sensing in environments unreachable by human beings which is essential for explosive detection. **Table 1–5** summarize the performance of some types of optical fiber sensors for the detection of glucose, pH, relative humidity (RH), gas, and ions, respectively. Among the discussed optical fiber sensors, FBGs function in both transmission and reflection configurations and because the reflection configuration does not require both ends of the fiber to be connected to the interrogation setup – this mode is more practical. Also, FBGs are immune to light source intensity fluctuation. FBGs is favorable for temperature detection due to the thermo-optic effect of the fiber core material induced by the temperature. Also, it is ideal for distributed strain monitoring as it is capable of the real-time monitoring of structures to assist in improving the safety of the structure by allowing timely repair which prevents the unwanted damages.

**Table 1.** Comparison of the performance for different kinds of optical fiber glucose sensors.

Fiber type	Glucose-responsive material	Detection range	LOD	References
EFBGs	4APBA-rGO	1 nM–10 mM	1 nM	[34a]
LPFG	GOD	0.56–166.67 mM	–	[42]
LPFG	(PEI/PAA)/GOD	1 nM–10 $\mu\text{M}$	1 nM	[127]
LPFG	GOD	0.1–3.2 mM	–	[128]
LPFG	GOD	0.0–166.67 mM	–	[29]
LPFG	GO/GOD	0–8 mM	–	[129]
LPFG	GOD	6.56–138.89 mM	1.11 mM	[130]
TOFI	GOD	0.0–166.67 mM	–	[131]
FPIF	PVA/P)AAm-AAPBA)	0–10 mM	–	[132]
FPIF	4-ANMP/PVC	1 $\mu\text{M}$ –1 M	–	[133]
SPR	GOD/PAAm	0–14.44 mM	–	[94]
SPR	GOD	0–138.89 mM	7.89 nM	[134]
FF	Con A and dextran	0–550 mg dL	–	[135]
FF	Con A and dextran	0–350 mg dL	–	[136]
LDOF	3-APBA	0–50 mM	–	[126b]

**Table 2.** Comparison for the performance of different kinds of optical fiber pH sensors.

Fiber type	pH-responsive material	Sensitivity [ $\text{nm pH}^{-1}$ ]	Detection range	Response time [s]	References
FBGs	PVA/PAA hydrogel	0.0122	2–7	$t_r = 200$ $t_f = 150$	[19]
FBGs	PNIPAM/SA/PEG hydrogel	0.0234 0.0143 0.014	1–4 5–9 10–14	$t = 80$	[20]
EFBGs	PAH/PAA hydrogel	0.3	1–3	–	[32]
TFBG	PANi	–	2–12	$t_r = 29$ $t_f = 67$	[137]
TFBG	PDDA/PAA hydrogel	–	4.66–6.02	$t_r = 10$ $t_f = 18$	[30]
LPFG	PAAm	0.66	2–12	$t = 2$	[138]
LPFG	PAA	7.5	2–7	$t_r = 100$ $t_f = 130$	[139]
LPFG	PVPON/PMAA hydrogel	–	2–7.5	–	[140]
LPFG	PAH/PAA hydrogel	8.74	4–7	–	[141]
TOFI	PVA/PAA hydrogel	1.58	2.48–6.47	$t_r = 10$ $t_f = 11$	[142]
FOMZI	Copolymer hydrogel	1.7	6.5–7.75	–	[143]
SPR	PAAm hydrogel	–	2–12	$t = 60$	[144]
SPR	PAAm hydrogel	13	8–10	$t = 20$	[93]
FF	Coumarin imidazole dye	–	10.0–13.2	$t = 50$ min	[145]
FF	FAM and <i>p</i> -THPP	–	5.5–8.0	$t = 30$	[119]

**Table 3.** Comparison of the performance of different kinds of optical fiber RH sensors.

Fiber type	RH-responsive material	Sensitivity	Detection range [%]	Response time [s]	References
TFBGs	PVA hydrogel	–	20–85	$t = 2$	[146]
TFBGs	GO	0.01	20–80	$t_r = 735$ $t_f = 1305$	[147]
LPFG	PAH/PAA hydrogel	0.063	20–80	–	[148]
FPIF	PVA hydrogel	–	35–95	$t = 0.5$	[149]
FPIF	Chitosan hydrogel	–	35–95	$t = 60$	[150]
FPIF	PI hydrogel	1.31	40–80	$t = 4$	[151]
FOMZI	SiO <sub>2</sub> NPs	–	26.5–83.8	–	[152]
SPR	Nafion film	3.78	30–85	$t = 0.5$	[153]
SPR	WS <sub>2</sub>	–	35–85	$t_r = 1$ $t_f = 5$	[154]
SPR	GO	0.145	32–85	$t_r = 2.73$ $t_f = 7.27$	[155]
FF	Approximately trapped in HPC	–	1.68–100	$t = 1–2$ min	[156]

However, for biosensing applications, the standard FBGs need to be modified to function conveniently. For example, for sensing glucose, the Bragg gratings segment needs to be etched or the gratings have to be made tilted. On the other side, LPFG has been proved to be not very sensitive to the change in the surrounding refractive index and its sensitivity needs to be enhanced to be suitable for biosensing applications too. However, it is easier

to be manufactured compared to FBGs and can be tuned to function in any electromagnetic spectrum range. LPFG is a good candidate for temperature and strain monitoring. The studies focus on developing tapered fiber lonely for sensing applications are relatively few compared to the other discussed fiber sensors because it offers low sensitivity, particularly when it is used for detecting small molecules, in addition to suffering poor mechanical properties in the tapered region. FPIF has been explored for the detection of glucose, pH, RH, gas, ions, and pressure. Among all these applications, FPIF is a promising tool for pressure and flow rate due to its superior performance and the capability to function in reflection mode. The studies showed that FOSI is a very promising tool for temperature detection over the FBGs and LPGs. Also, FOSI is quite sensitive to the local refractive change compared with the other discussed fiber sensors; however, its bulky structure is a considerable barrier to being used for many applications. SPR-based fiber sensors showed to be beneficial for numerous applications; however, its sensitivity for small molecules is quite low. Using graphene, silicon, and other materials with the plasmonic layer proved to be an effective strategy to overcome these shortcomings. Also, tapering and bending the SPR-based fiber sensors have been found to improve their sensitivity and make it capable of detecting even the small molecules. The previous studies showed that SPR-based fiber sensors are promising candidates for practical detection of metabolites, biomarkers, viruses, bacteria, cancer, pH, gases, ions, and relative humidity. Fluorescent fiber sensors are quite sensitive and able to provide a very low limit of detection. Their applications span from biomedicine to environment. A few examples of the fluorescence-based sensors used for monitoring glucose, pH, relative humidity, gas, and ions, are displayed in the provided Table 1–5. Up till now, LDOF sensors have been explored only for the detection of

**Table 4.** Comparison for the performance of different kinds of optical fiber gas sensors.

Fiber Type	Gas-responsive material	Gas type	Detection range	LOD	References
FBGs	Pd	H <sub>2</sub>	0–10%	–	[33]
FBGs	Pd-NPs	H <sub>2</sub>	0–10%	–	[157]
EFBGs	Pd/Ni	H <sub>2</sub>	0–4%	–	[158]
LPFG	Pd	H <sub>2</sub>	0–4%	–	[159]
LPFG	(PDDA/SiO <sub>2</sub> )/TSP	NH <sub>3</sub>	0.1–10 ppm	140 ppb	[160]
LPFG	PAH/PAA	NH <sub>3</sub>	0–348 ppm	10.7 ppm	[161]
TOFI	Silica gels	NH <sub>3</sub>	0–40 ppm	5 ppb	[162]
FPIF	Pd	H <sub>2</sub>	0–8%	–	[163]
FPIF	Pd-Y film	H <sub>2</sub>	0–5.5%	–	[164]
FPIF	PDMS	EtOH	0–6800 ppm	–	[165]
FPIF	PEI/PVA hydrogel	CO <sub>2</sub>	0–86.9%	–	[166]
FPIF	PAVB hydrogel	CO <sub>2</sub>	0–75%	286 ppm	[167]
SPR	BCP	NH <sub>3</sub>	0–150 ppm	–	[168]
SPR	Cu–ZnO thin film	H <sub>2</sub> S	0–100 ppm	–	[169]
SPR	GCNT/PMMA nanocomposite	CH <sub>4</sub>	0–100 ppm	–	[170]
SPR	NiO-ITO	H <sub>2</sub> S	0–100	–	[171]
FF	Ferrous core–shell NPs and Rhodamine B	NH <sub>3</sub>	0–12 000 ppm	–	[172]
FF	AQmol-2	Nerve agents (DFP and DCP)	–	0.16 $\mu$ M and 0.18 $\mu$ M	[173]

**Table 5.** Comparison of the performance of different kinds of optical fiber ion sensors.

Fiber type	Ion-responsive material	Ion type	Detection range	LOD	References
FBGs	PATAC hydrogel	Cr <sup>6+</sup>	10–100 ppb mm	10 ppb	[22]
EFBGs	PATAC hydrogel	Cr <sup>6+</sup>	0–100 mm	10 ppb	[174]
FF	Si QDs	Cr <sup>6+</sup>	1.25–40 μm	0.65 μm	[175]
FF	CdSe QDs	Cr <sup>3+</sup>	0.1–20 μm	–	[175]
TFBGs	BP	Pb <sup>2+</sup>	0.1–1.5 × 10 <sup>7</sup> ppb	0.25 ppb	[31]
TOFI	EDTA	Cd <sup>2+</sup>	0–1000 ppb	10 ppb	[176]
FF	Metal chelating moieties (DPA)	Cd <sup>2+</sup>	–	–	[177]

glucose, pH, and alcohols, and their performance is summarized in the provided Table 1–2.

## 10. Conclusion and Future Prospects

Fiber-optic probes based on different sensing mechanisms were discussed. Brief theory, fabrication processes, readout methodologies, sensing principles, and limitations of the fiber probes were addressed. However research on fiber-optic probes started 30 years ago, and few types of optical fiber probes reached the commercialization stage such as fiber Bragg gratings that are used in real-time monitoring of deformation in constructions, aircraft, and ships. Currently, fiber-optic probes based on the Fabry–Pérot interferometer are available in the market for applications such as temperature measurements, which are developed by OMEGA. Also, Fabry–Pérot fiber probes for continuous glucose detection may have application in intensive-care units shortly as it is currently under development by Glucoset. Fluorescence-based fiber probes are valuable for many applications and reached the commercialization stage for applications such as pH sensing which was developed by pH Optica micro. However, fluorescent fiber probes are adversely affected by the photobleaching of fluorophores. Optical fiber integrated-light diffuser probes emerged in 2019 as a promising technology due to their compact design configuration and robust performance; however, it does require a light source of stable output.

The market for fiber-optic sensors has been growing very slowly to compete with the conventional sensor technology since 1980. Considering the projection of the fiber-optic sensors market in 2020 and the evolution in fiber-optic manufacturing, it is expected that the fiber-optic sensors to be cost-effective and attractive due to their inherent advantages such as the immunity to electromagnetic interference, compact size, and the light-weight. So, the trend of the fiber-optic probes is to ease the fabrication to be applicable for mass production and to simplify the readout methodology, in addition to overcoming the challenges related to sensitivity, response time, repeatability, and reusability, and find alternatives for the bulky and costly instruments for developing handy-held, portable probes that can be used in-site.

## Acknowledgements

The authors acknowledge Khalifa University of Science and Technology (KUST) and KU-KAIST Joint Research Center for research funding in

support on this research (Project code: 8474000220-KKJRC-2019-Health1). H.B. acknowledges Sandooq Al Watan LLC and Aldar Properties for the joint research funding (SWARD Program - AWARD Ref. SWARD-F19-008).

## Conflict of Interest

The authors declare no conflict of interest.

## Keywords

diffraction, fiber-optic sensors, fluorescence, interferometry, light diffusion, surface plasmon resonance

Received: December 20, 2021

Revised: June 3, 2022

Published online:

- [1] J. M. Senior, M. Y. Jamro, *Optical Fiber Communications: Principles and Practice*, Pearson Education, Harlow, England **2009**.
- [2] A. Arie, R. Karoubi, Y. S. Gur, M. Tur, *Appl. Opt.* **1986**, 25, 1754.
- [3] J. M. Coelho, C. Silva, M. Nespereira, M. Abreu, J. Rebordão, *Advances in Optical Fiber Technology: Fundamental Optical Phenomena and Applications*, IntechOpen, London, UK **2015**, p. 287.
- [4] S. Zhu, F. Pang, S. Huang, F. Zou, Q. Guo, J. Wen, T. Wang, *Sensors* **2016**, 16, 1295.
- [5] C. M. Davis, *Opt. Eng.* **1985**, 24, 242347.
- [6] I.-L. Bundalo, K. Nielsen, G. Woyessa, O. Bang, *Opt. Mater. Express* **2017**, 7, 967.
- [7] M. A. Riza, Y. I. Go, S. W. Harun, R. R. Maier, *IEEE Sens. J* **2020**, 20, 7614.
- [8] S. Yin, P. Ruffin, *Wiley Encyclopedia of Biomedical Engineering*, Wiley, Hoboken, NJ, USA **2006**.
- [9] P. Delaney, M. Harris, *Handbook of Biological Confocal Microscopy*, Springer, Boston, MA, USA **2006**.
- [10] X.-D. Wang, O. S. Wolfbeis, *Anal. Chem.* **2019**, 92, 397.
- [11] a) G. Kostovski, P. R. Stoddart, A. Mitchell, *Adv. Mater.* **2014**, 26, 3798; b) J. S. Paiva, P. A. Jorge, C. C. Rosa, J. P. Cunha, *Biochim. Biophys. Acta, Gen. Subj.* **2018**, 1862, 1209.
- [12] P. Vaiano, B. Carotenuto, M. Pisco, A. Ricciardi, G. Quero, M. Consales, A. Crescitelli, E. Esposito, A. Cusano, *Laser Photonics Rev.* **2016**, 10, 922.
- [13] a) M. McSherry, C. Fitzpatrick, E. Lewis, *Sens. Rev.* **2005**, 25, 56; b) C. Merzbacher, A. D. Kersey, E. Friebele, *Smart Mater. Struct.* **1996**, 5, 196; c) Y. Bao, Y. Huang, M. S. Hoehler, G. Chen, *Sensors* **2019**, 19, 877; d) C. Du, S. Dutta, P. Kurup, T. Yu,

- X. Wang, *Sens. Actuators, A* **2020**, *303*, 111728; e) B. H. Lee, Y. H. Kim, K. S. Park, J. B. Eom, M. J. Kim, B. S. Rho, H. Y. Choi, *Sensors* **2012**, *12*, 2467; f) A. K. Sharma, R. Jha, B. Gupta, *IEEE Sens. J.* **2007**, *7*, 1118; g) Y. Chen, H. Ming, *Photonics Sens.* **2012**, *2*, 37; h) K. A. Tomyshev, D. K. Tazhetdinova, E. S. Manuilovich, O. V. Butov, *J. Appl. Phys.* **2018**, *124*, 113106; i) Y. Zhao, R.-J. Tong, F. Xia, Y. Peng, *Biosens. Bioelectron.* **2019**, *142*, 111505; j) Y. Liu, W. Peng, *J. Lightwave Technol.* **2021**, *39*, 3781; k) P. Gong, X. Li, X. Zhou, Y. Zhang, N. Chen, S. Wang, S. Zhang, Y. Zhao, *Opt. Laser Technol.* **2021**, *139*, 106981; l) E. Benito-Peña, M. G. Valdés, B. Glahn-Martínez, M. C. Moreno-Bondi, *Anal. Chim. Acta* **2016**, *943*, 17; m) C. Broadway, R. Min, A. G. Leal-Junior, C. Marques, C. Caucheteur, *J. Lightwave Technol.* **2019**, *37*, 2605; n) D. Tosi, *Sensors* **2018**, *18*, 2147; o) X.-W. Zhao, Q. Wang, *Instrum. Sci. Technol.* **2019**, *47*, 140; p) S. Korposh, S. W. James, S.-W. Lee, R. P. Tatam, *Sensors* **2019**, *19*, 2294; q) Z. Ding, C. Wang, K. Liu, J. Jiang, D. Yang, G. Pan, Z. Pu, T. Liu, *Sensors* **2018**, *18*, 1072; r) A. K. Sharma, A. K. Pandey, B. Kaur, *Opt. Fiber Technol.* **2018**, *43*, 20; s) N. Cennamo, M. Pesavento, L. Zeni, *Sens. Actuators, B* **2021**, *331*, 129393.
- [14] a) I. Vitoria, C. Ruiz Zamarreño, A. Ozcariz, I. R. Matias, *Sensors* **2021**, *21*, 731; b) V. Portosi, D. Laneve, M. C. Falconi, F. Prudenziario, *Sensors* **2019**, *19*, 1892; c) P. A. Mosier-Boss, *Nanomaterials* **2017**, *7*, 142; d) P. Lu, N. Lalam, M. Badar, B. Liu, B. T. Chorpening, M. P. Buric, P. R. Ohodnicki, *Appl. Phys. Rev.* **2019**, *6*, 041302; e) J. Villatoro, J. Zubia, *Opt. Laser Technol.* **2016**, *78*, 67; f) E. Udd, *Rev. Sci. Instrum.* **1995**, *66*, 4015.
- [15] R. Kashyap, *Fiber Bragg Gratings*, Academic Press, London, UK **2009**.
- [16] M. Kreuzer, *Strain Measurement with Fiber Bragg Grating Sensors*, S2338-1.0 e, HBM, Darmstadt **2006**, p. 12.
- [17] a) J. Canning, *Laser Photonics Rev.* **2008**, *2*, 275; b) Y.-J. Rao, *Meas. Sci. Technol.* **1997**, *8*, 355; c) A. D. Kersey, M. A. Davis, H. J. Patrick, M. LeBlanc, K. Koo, C. Askins, M. Putnam, E. J. Friebele, *J. Lightwave Technol.* **1997**, *15*, 1442; d) J.-M. Renoirt, C. Caucheteur, M. Olivier, P. Mégret, M. Debliquy, in *Infrared Radiation*, IntechOpen, Rijeka, Croatia **2012**.
- [18] A. Theodosiou, P. Savva, E. Mendoza, M. Petrou, K. Kalli, *IEEE Sens. J.* **2021**, *21*, 16086.
- [19] V. N. K. Pabbiseti, S. S. Madhvarasu, *Opt. Eng.* **2016**, *55*, 066112.
- [20] Y. Lin, M. Wang, W. Liu, *Opt. Eng.* **2015**, *54*, 057107.
- [21] M.-J. Yin, B. Gu, Q.-F. An, C. Yang, Y. L. Guan, K.-T. Yong, *Coord. Chem. Rev.* **2018**, *376*, 348.
- [22] P. Kishore, M. S. Shankar, M. Satyanarayana, *Sens. Actuators, B* **2017**, *243*, 626.
- [23] Y. Zhao, Q.-L. Wu, Y.-N. Zhang, *IEEE Trans. Instrum. Meas.* **2017**, *66*, 2198.
- [24] B. Sutapun, M. Tabib-Azar, A. Kazemi, *Sens. Actuators, B* **1999**, *60*, 27.
- [25] X.-D. Wang, O. S. Wolfbeis, *Anal. Chem.* **2013**, *85*, 487.
- [26] E. Udd, *Fiber Optic Smart Structures (A 95-34976 09-39)*, John Wiley & Sons, Inc. (Wiley Series in Pure and Applied Optics), New York, NY **1995**, p. 5.
- [27] B. Lee, Y. Jeong, S. Yin, P. Ruffin, F. Yu, *Interrogation Techniques for Fiber Grating Sensors and the Theory Of Fiber Gratings*, CRC Press, Boca Raton, FL **2008**.
- [28] T. Klotz, R. Pothier, D. Walch, T. Colombo, *Results Eng.* **2021**, *9*, 100190.
- [29] B. Luo, Z. Yan, Z. Sun, J. Li, L. Zhang, *Opt. Express* **2014**, *22*, 30571.
- [30] L.-Y. Shao, M.-J. Yin, H.-Y. Tam, J. Albert, *Sensors* **2013**, *13*, 1425.
- [31] C. Liu, Z. Sun, L. Zhang, J. Lv, X. Yu, X. Chen, *Sens. Actuators, B* **2018**, *257*, 1093.
- [32] B. Shivananju, G. Prashanth, S. Asokan, M. M. Varma, *Sens. Actuators, B* **2014**, *201*, 37.
- [33] S. Silva, L. Coelho, J. Almeida, O. Frazão, J. L. Santos, F. Malcata, M. Becker, M. Rothhardt, H. Bartelt, *IEEE Photonics Technol. Lett.* **2013**, *25*, 401.
- [34] a) S. Sridevi, K. Vasu, S. Sampath, S. Asokan, A. Sood, *J. Biophotonics* **2016**, *9*, 760; b) S. Sridevi, K. Vasu, S. Asokan, A. Sood, *Biosens. Bioelectron.* **2015**, *65*, 251.
- [35] S. Iacoponi, C. Massaroni, D. L. Presti, P. Saccomandi, M. A. Caponero, R. D'Amato, E. Schena, in *presented at 2018 40th Annual Inter. Conf. of the IEEE Engineering in Medicine and Biology Society (EMBC)*, IEEE, Honolulu, HI, USA **2018**.
- [36] A. Iadicicco, S. Campopiano, A. Cutolo, M. Giordano, A. Cusano, *Sens. Actuators, B* **2006**, *120*, 231.
- [37] A. Iadicicco, A. Cusano, A. Cutolo, R. Bernini, M. Giordano, *IEEE Photonics Technol. Lett.* **2004**, *16*, 1149.
- [38] S. W. James, R. P. Tatam, *Meas. Sci. Technol.* **2003**, *14*, R49.
- [39] C. Silva, J. M. Coelho, P. Caldas, P. Jorge, *Fiber Optic Sensors*, IntechOpen, Rijeka, Croatia **2012**.
- [40] V. Bhatia, A. M. Vengsarkar, *Opt. Lett.* **1996**, *21*, 692.
- [41] J. M. Corres, I. R. Matias, I. del Villar, F. J. Arregui, *IEEE Sens. J.* **2007**, *7*, 455.
- [42] A. Deep, U. Tiwari, P. Kumar, V. Mishra, S. C. Jain, N. Singh, P. Kapur, L. M. Bharadwaj, *Biosens. Bioelectron.* **2012**, *33*, 190.
- [43] B. Xu, J. Huang, L. Ding, J. Cai, *Mater. Sci. Eng., C* **2020**, *107*, 110329.
- [44] M. Janczuk-Richter, B. Gromadzka, Ł. Richter, M. Panasiuk, K. Zimmer, P. Mikulic, W. J. Bock, S. Maćkowski, M. Śmietana, J. Niedziółka Jönsson, *Sensors* **2020**, *20*, 813.
- [45] F. Esposito, L. Sansone, A. Srivastava, F. Baldini, S. Campopiano, F. Chiaiaoli, M. Giordano, A. Giannetti, A. Iadicicco, *Biosens. Bioelectron.* **2021**, *172*, 112747.
- [46] M. I. Zibaii, A. Kazemi, H. Latifi, M. K. Azar, S. M. Hosseini, M. H. Ghezelaiaigh, *J. Photochem. Photobiol., B* **2010**, *101*, 313.
- [47] A. W. Snyder, J. Love, *Optical Waveguide Theory*, Springer Science & Business Media, New York, USA **2012**.
- [48] W. Stewart, *IOOC-ECOC '85: 5th International Conference on Integrated Optics and Optical Fibre Communication: 11th European Conference on Optical Communication: Venezia, Italy, October 1-4, 1985: technical digest*, Istituto Internazionale Delle Comunicazioni, Genova, Italy **1985**, <https://www.worldcat.org/title/iooc-ecoc-85-5th-international-conference-on-integrated-optics-and-optical-fibre-communication-11th-european-conference-on-optical-communication-venezia-italy-october-1-4-1985-technical-digest/oclc/80475995>.
- [49] L. Chen, Y.-K. Leng, B. Liu, J. Liu, S.-P. Wan, T. Wu, J. Yuan, L. Shao, G. Gu, Y. Q. Fu, *Sens. Actuators, B* **2020**, *320*, 128283.
- [50] H. Qiu, S. Xu, S. Jiang, Z. Li, P. Chen, S. Gao, C. Zhang, D. Feng, *Appl. Surf. Sci.* **2015**, *329*, 390.
- [51] Z.-H. Wu, Q. Wang, J.-X. Duan, H.-Z. Sun, Q. Zhao, *Instrum. Sci. Technol.* **2021**, *49*, 32.
- [52] C. Deng, K. Hansen, J. Haus, P. P. Banerjee, U. Sinha, in *presented at Optical Fibers and Sensors for Medical Diagnostics and Treatment Applications XX*, Society of Photo-Optical Instrumentation Engineers (SPIE), San Francisco, CA, USA **2020**.
- [53] B.-H. Lee, J.-B. Eom, K.-S. Park, S.-J. Park, M.-J. Ju, *J. Opt. Soc. Korea* **2010**, *14*, 326.
- [54] K. T. Grattan, B. T. Meggitt, *Optical Fiber Sensor Technology*, Vol. 1, Springer, New York, USA **1995**.
- [55] J. Sirkis, D. Brennan, M. Putman, T. Berkoff, A. Kersey, E. Friebele, *Opt. Lett.* **1993**, *18*, 1973.
- [56] a) W.-H. Tsai, C.-J. Lin, *J. Lightwave Technol.* **2001**, *19*, 682; b) J. J. Lee, S. H. Kim, D. C. Lee, I. B. Kwon, Google Patents **2004**; c) S.-H. Kim, J.-J. Lee, D.-C. Lee, I.-B. Kwon, *J. Lightwave Technol.* **1999**, *17*, 1869
- [57] K. Koo, M. LeBlanc, T. Tsai, S. Vohra, *IEEE Photonics Technol. Lett.* **1998**, *10*, 1006.

- [58] a) J. S. Santos, I. M. Raimundo Jr, C. M. Cordeiro, C. R. Biazoli, C. A. Gouveia, P. A. Jorge, *Sens. Actuators, B* **2014**, 196, 99; b) W. Xu, W.-B. Huang, X.-G. Huang, C.-Y. Yu, *Opt. Fiber Technol.* **2013**, 19, 583; c) S. Tierney, D. R. Hjelm, B. T. Stokke, *Anal. Chem.* **2008**, 80, 5086; d) S. Tierney, B. M. H. Falch, D. R. Hjelm, B. T. Stokke, *Anal. Chem.* **2009**, 81, 3630.
- [59] S. Tierney, S. Volden, B. T. Stokke, *Biosens. Bioelectron.* **2009**, 24, 2034.
- [60] J. Goicoechea, C. Zamarreño, I. Matias, F. Arregui, *Sens. Actuators, B* **2009**, 138, 613.
- [61] P. Thaisongkroh, S. Pullteap, H. C. Seat, *Eng. J.* **2021**, 25, 317.
- [62] W. Huang, Z. Zhang, J. He, B. Du, C. Liao, S. Liu, G. Yin, Y. Wang, *Sensors* **2020**, 20, 2548.
- [63] B. Kim, H. Jeong, Y. S. Lee, S. Hong, K. Oh, *Sens. Actuators Rep.* **2021**, 3, 100038.
- [64] J. Han, D. P. Neikirk, in *presented at Micromachined Devices and Components II*, Society of Photo-Optical Instrumentation Engineers (SPIE), Austin, TX, United States **1996**.
- [65] a) J. H. Lim, H. S. Jang, K. S. Lee, J. C. Kim, B. H. Lee, *Opt. Lett.* **2004**, 29, 346; b) Y.-J. Kim, U.-C. Paek, B. H. Lee, *Opt. Lett.* **2002**, 27, 1297; c) T. Allsop, R. Reeves, D. J. Webb, I. Bennion, R. Neal, *Rev. Sci. Instrum.* **2002**, 73, 1702; d) Y.-H. Kim, M.-J. Kim, M.-S. Park, J.-H. Jang, B.-H. Lee, K.-T. Kim, *J. Opt. Soc. Korea* **2008**, 12, 221; e) M. Kim, Y. Kim, G. Mudhana, B. Lee, *IEEE Photonics Technol. Lett.* **2008**, 20, 1290; f) J.-F. Ding, A. P. Zhang, L.-Y. Shao, J.-H. Yan, S. He, *IEEE Photonics Technol. Lett.* **2005**, 17, 1247.
- [66] B. H. Lee, U.-C. Paek, *J. Lightwave Technol.* **2002**, 20, 1750.
- [67] T. Hao, K. S. Chiang, *IEEE Photonics Technol. Lett.* **2017**, 29, 2035.
- [68] X. Fan, Q. Wang, M. Zhou, F. Liu, H. Shen, Z. Wei, F. Wang, C. Tan, H. Meng, *Opt. Express* **2020**, 28, 24682.
- [69] a) D. W. Kim, Y. Zhang, K. L. Cooper, A. Wang, *Appl. Opt.* **2005**, 44, 5368; b) A. Van Brakel, P. L. Swart, *Opt. Eng.* **2005**, 44, 020504; c) L. Yuan, J. Yang, Z. Liu, *IEEE Sens. J.* **2008**, 8, 1114.
- [70] D. Liu, Y. Xie, G. Xin, Z.-Y. Li, *Sens. Transducers* **2013**, 160, 215.
- [71] P. Fan, W. Yan, P. Lu, W. Zhang, W. Zhang, X. Fu, J. Zhang, *Opt. Express* **2020**, 28, 25238.
- [72] M. Stolarik, J. Nedoma, R. Martinek, S. Kepak, E. Hrubesova, M. Pinka, J. Kolarik, *Photonics* **2021**, 8, 147.
- [73] Y. Zhang, Y. Guo, F. Zhu, K. Qi, in *presented at Optical and Quantum Sensing and Precision Metrology*, Society of Photo-Optical Instrumentation Engineers (SPIE) **2021**, <https://doi.org/10.1117/12.2586523>.
- [74] H. Fu, H. Tam, L.-Y. Shao, X. Dong, P. Wai, C. Lu, S. K. Khijwania, *Appl. Opt.* **2008**, 47, 2835.
- [75] a) D. S. Moon, B. H. Kim, A. Lin, G. Sun, Y.-G. Han, W.-T. Han, Y. Chung, *Opt. Express* **2007**, 15, 7962; b) G. Kim, T. Cho, K. Hwang, K. Lee, K. S. Lee, Y.-G. Han, S. B. Lee, *Opt. Express* **2009**, 17, 2481; c) A. Starodumov, L. Zenteno, D. Monzon, E. De La Rosa, *Appl. Phys. Lett.* **1997**, 70, 19.
- [76] E. Reyes-Vera, C. M. Cordeiro, P. Torres, *Appl. Opt.* **2017**, 56, 156.
- [77] H. Fu, H. Y. Tam, L.-Y. Shao, X. Dong, P. K. A. Wai, C. Lu, S. K. Khijwania, *Appl. Opt.* **2008**, 47, 2835.
- [78] M. A. Mollah, R. J. Usha, S. Tasnim, K. Ahmed, *Opt. Quantum Electron.* **2020**, 52, 1.
- [79] R. W. Wood, *London, Edinburgh Dublin Philos. Mag. J. Sci.* **1902**, 4, 396.
- [80] U. Fano, *JOSA* **1941**, 31, 213.
- [81] A. Vinogradov, A. Dorofeenko, A. Pukhov, A. Lisiansky, *Phys. Rev. B* **2018**, 97, 235407.
- [82] J. Jana, M. Ganguly, T. Pal, *RSC Adv.* **2016**, 6, 86174.
- [83] J. Wu, Y. Yan, S. Li, X. Ding, S. Ding, Y. Huang, *Meas. Sci. Technol.* **2015**, 26, 105701.
- [84] H. Raether, *Surface Plasmons on Smooth and Rough Surfaces and on Gratings*, Springer, Berlin, Heidelberg, Germany **1988**.
- [85] B. D. Gupta, R. Kant, *Opt. Laser Technol.* **2018**, 101, 144.
- [86] a) V. Myroshnychenko, J. Rodríguez-Fernández, I. Pastoriza-Santos, A. M. Funston, C. Novo, P. Mulvaney, L. M. Liz-Marzan, F. J. G. de Abajo, *Chem. Soc. Rev.* **2008**, 37, 1792; b) S. Unser, I. Bruzas, J. He, L. Sagle, *Sensors* **2015**, 15, 15684.
- [87] W. H. Yang, G. C. Schatz, R. P. Van Duyne, *J. Chem. Phys.* **1995**, 103, 869.
- [88] J. Cao, T. Sun, K. T. Grattan, *Sens. Actuators, B* **2014**, 195, 332.
- [89] L. S. Jung, C. T. Campbell, T. M. Chinowsky, M. N. Mar, S. S. Yee, *Langmuir* **1998**, 14, 5636.
- [90] a) P. B. Johnson, R.-W. Christy, *Phys. Rev. B* **1972**, 6, 4370; b) P. R. West, S. Ishii, G. V. Naik, N. K. Emani, V. M. Shalaev, A. Boltasseva, *Laser Photonics Rev.* **2010**, 4, 795.
- [91] A. Leung, P. M. Shankar, R. Mutharasan, *Sens. Actuators, B* **2007**, 125, 688.
- [92] M. Iga, A. Seki, K. Watanabe, *Sens. Actuators, B* **2004**, 101, 368.
- [93] Y. Zhao, M. Lei, S.-X. Liu, Q. Zhao, *Sens. Actuators, B* **2018**, 261, 226.
- [94] S. Singh, B. D. Gupta, *Sens. Actuators, B* **2013**, 177, 589.
- [95] B. Du, Y. Ruan, T.-T. Ly, P. Jia, Q. Sun, Q. Feng, D. Yang, H. Ebendorff-Heidepriem, *Sens. Actuators, B* **2020**, 305, 127513.
- [96] S. K. Srivastava, V. Arora, S. Sapra, B. D. Gupta, *Plasmonics* **2012**, 7, 261.
- [97] S. Kaushik, U. K. Tiwari, S. S. Pal, R. K. Sinha, *Biosens. Bioelectron.* **2019**, 126, 501.
- [98] M. Loyez, M. Lobry, E. M. Hassan, M. C. DeRosa, C. Caucheteur, R. Wattiez, *Talanta* **2021**, 221, 121452.
- [99] C. Leitão, A. Leal-Junior, A. R. Almeida, S. O. Pereira, F. M. Costa, J. L. Pinto, C. Marques, *Biotechnol. Rep.* **2021**, 29, e00587.
- [100] a) Y. Ying, G.-Y. Si, F.-J. Luan, K. Xu, Y.-W. Qi, H.-N. Li, *Opt. Laser Technol.* **2017**, 90, 149; b) K. Gasior, T. Martynkien, M. Napiorkowski, K. Zolnaczyk, P. Mergo, W. Urbanczyk, *J. Opt.* **2016**, 19, 025001; c) S. Weng, L. Pei, J. Wang, T. Ning, J. Li, *Photonics Res.* **2017**, 5, 103; d) M. Irigoyen, J. A. Sánchez-Martin, E. Bernabeu, A. Zamora, *Meas. Sci. Technol.* **2017**, 28, 045802.
- [101] H. Yuan, W. Ji, S. Chu, S. Qian, F. Wang, J.-F. Masson, X. Han, W. Peng, *Biosens. Bioelectron.* **2018**, 117, 637.
- [102] T. Xie, Y. He, Y. Yang, H. Zhang, Y. Xu, *Plasmonics* **2021**, 16, 205.
- [103] H. Manoharan, K. Dharanibalaji, V. Sai, *Plasmonics* **2021**, 1, 1307.
- [104] M. Divagar, R. Bandaru, V. Janakiraman, V. Sai, *Biosens. Bioelectron.* **2020**, 167, 112488.
- [105] A. George, M. Amrutha, P. Srivastava, S. Sunil, V. Sai, R. Srinivasan, *Analyst* **2021**, 146, 244.
- [106] Y.-C. Kim, S. Banerji, J.-F. Masson, W. Peng, K. S. Booksh, *Analyst* **2005**, 130, 838.
- [107] Q. Ouyang, S. Zeng, L. Jiang, L. Hong, G. Xu, X.-Q. Dinh, J. Qian, S. He, J. Qu, P. Coquet, *Sci. Rep.* **2016**, 6, 1.
- [108] D. C. Klonoff, *J. Diabetes Sci. Technol.* **2012**, 6, 1242.
- [109] R. Williams, J. Bridges, *J. Clin. Pathol.* **1964**, 17, 371.
- [110] P. Kaláb, J. Soderholm, *Methods* **2010**, 51, 220.
- [111] A. R. Clapp, I. L. Medintz, H. Mattoussi, *ChemPhysChem* **2006**, 7, 47.
- [112] G. Springsteen, B. Wang, *Chem. Commun.* **2001**, 1608.
- [113] H. Cao, D. I. Diaz, N. DiCesare, J. R. Lakowicz, M. D. Heagy, *Org. Lett.* **2002**, 4, 1503.
- [114] D. C. Klonoff, *J. Diabetes Sci. Technol.* **2012**, 6, 1242.
- [115] Y. J. Heo, H. Shibata, T. Okitsu, T. Kawanishi, S. Takeuchi, *Proc. Natl. Acad. Sci.* **2011**, 108, 13399.
- [116] a) L. Bilro, N. Alberto, J. L. Pinto, R. Nogueira, *Sensors* **2012**, 12, 12184; b) Y. Koike, K. Koike, *J. Polym. Sci., Part B: Polym. Phys.* **2011**, 49, 2.
- [117] H. Shibata, Y. J. Heo, T. Okitsu, Y. Matsunaga, T. Kawanishi, S. Takeuchi, *Proc. Natl. Acad. Sci.* **2010**, 107, 17894.
- [118] M. Shortreed, R. Kopelman, M. Kuhn, B. Hoyland, *Anal. Chem.* **1996**, 68, 1414.

- [119] J. Gong, M. G. Tanner, S. Venkateswaran, J. M. Stone, Y. Zhang, M. Bradley, *Anal. Chim. Acta* **2020**, *1134*, 136.
- [120] A. Tariq, J. Baydoun, C. Remy, R. Ghasemi, J. P. Lefevre, C. Mongin, A. Dauzères, I. Leray, *Sens. Actuators, B* **2021**, *327*, 128906.
- [121] Q.-D. Huang, C.-H. Lv, X.-L. Yuan, M. He, J.-P. Lai, H. Sun, *Sens. Actuators, B* **2021**, *328*, 129000.
- [122] Y. Liu, X. Tang, M. Deng, T. Zhu, L. Edman, J. Wang, *J. Alloys Compd.* **2021**, *864*, 158109.
- [123] Y. Liu, X. Tang, W. Huang, G. Yin, M. Deng, Y. Cao, L. Shi, T. Zhu, L. Huang, I. P. Ikehukwu, *Microchim. Acta* **2020**, *187*, 1.
- [124] Z. Zhou, M. Shang, Z. Yao, J. Zhang, *Dyes Pigm.* **2022**, *198*, 110016.
- [125] A. K. Yetisen, N. Jiang, A. Fallahi, Y. Montelongo, G. U. Ruiz-Esparza, A. Tamayol, Y. S. Zhang, I. Mahmood, S. A. Yang, K. S. Kim, *Adv. Mater.* **2017**, *29*, 1606380.
- [126] a) M. Elsherif, R. Moreddu, M. U. Hassan, A. K. Yetisen, H. Butt, *Lab. Chip* **2019**, *19*, 2060; b) M. Elsherif, M. U. Hassan, A. K. Yetisen, H. Butt, *Biosens. Bioelectron.* **2019**, *137*, 25.
- [127] M.-J. Yin, B. Huang, S. Gao, A. P. Zhang, X. Ye, *Biomed. Opt. Express* **2016**, *7*, 2067.
- [128] A. A. Badmos, Q. Sun, Z. Sun, J. Zhang, Z. Yan, P. Lutsyk, A. Rozhin, L. Zhang, *J. Biomed. Opt.* **2017**, *22*, 027003.
- [129] B. Jiang, K. Zhou, C. Wang, Q. Sun, G. Yin, Z. Tai, K. Wilson, J. Zhao, L. Zhang, *Sens. Actuators, B* **2018**, *254*, 1033.
- [130] B. Luo, Z. Yan, Z. Sun, Y. Liu, M. Zhao, L. Zhang, *Opt. Express* **2015**, *23*, 32429.
- [131] Y. Li, H. Ma, L. Gan, Q. Liu, Z. Yan, D. Liu, Q. Sun, *Sens. Actuators B* **2018**, *255*, 3004.
- [132] X. Zhang, Y. Guan, Y. Zhang, *Biomacromolecules* **2012**, *13*, 92.
- [133] M. R. R. Khan, A. V. Watekar, S.-W. Kang, *IEEE Sens. J.* **2017**, *18*, 1528.
- [134] Y. Yuan, X. Yang, D. Gong, F. Liu, W. Hu, W. Cai, J. Huang, M. Yang, *Opt. Express* **2017**, *25*, 3884.
- [135] A. J. Müller, M. Knuth, K. S. Nikolaus, R. Krivánek, F. Küster, C. Hasslacher, SAGE Publications Sage CA, Los Angeles, CA **2013**.
- [136] R. Dutt-Ballerstadt, C. Evans, A. P. Pillai, E. Orzeck, R. Drabek, A. Gowda, R. McNichols, *J. Diabetes Sci. Technol.* **2012**, *6*, 362.
- [137] A. L. Aldaba, Á. González-Vila, M. Debligny, M. Lopez-Amo, C. Caucheteur, D. Lahem, *Sens. Actuators, B* **2018**, *254*, 1087.
- [138] S. K. Mishra, B. Zou, K. S. Chiang, *IEEE J. Sel. Top. Quantum Electron.* **2016**, *23*, 284.
- [139] M. J. Yin, M. Yao, S. Gao, A. P. Zhang, H. Y. Tam, P. K. A. Wai, *Adv. Mater.* **2016**, *28*, 1394.
- [140] F. Tian, J. Kanka, S. A. Sukhishvili, H. Du, *Opt. Lett.* **2012**, *37*, 4299.
- [141] I. Del Villar, M. Partridge, W. E. Rodriguez, O. Fuentes, A. B. Socorro, S. Diaz, J. M. Corres, S. W. James, R. P. Tatam, *Sensors* **2017**, *17*, 2094.
- [142] W. C. Wong, C. C. Chan, P. Hu, J. R. Chan, Y. T. Low, X. Dong, K. C. Leong, *Sens. Actuators, B* **2014**, *191*, 579.
- [143] Z. Q. Tou, C. C. Chan, J. Hong, S. Png, K. M. T. Eddie, T. A. H. Tan, *J. Biomed. Opt.* **2014**, *19*, 047002.
- [144] S. Singh, B. D. Gupta, *Sens. Actuators, B* **2012**, *173*, 268.
- [145] T. H. Nguyen, T. Venugopala, S. Chen, T. Sun, K. T. Grattan, S. E. Taylor, P. M. Basheer, A. E. Long, *Sens. Actuators, B* **2014**, *191*, 498.
- [146] J. Yang, X. Dong, K. Ni, C. C. Chan, P. P. Shun, *Appl. Opt.* **2015**, *54*, 2620.
- [147] Y.-D. Chiu, C.-W. Wu, C.-C. Chiang, *Sensors* **2017**, *17*, 2129.
- [148] A. Urrutia, J. Goicoechea, A. L. Ricchiuti, D. Barrera, S. Sales, F. J. Arregui, *Sens. Actuators, B* **2016**, *227*, 135.
- [149] H. Sun, X. Zhang, L. Yuan, L. Zhou, X. Qiao, M. Hu, *IEEE Sens. J.* **2014**, *15*, 2891.
- [150] X. Liu, M. Jiang, Q. Sui, X. Geng, *J. Mod. Opt.* **2016**, *63*, 1668.
- [151] C. Bian, M. Hu, R. Wang, T. Gang, R. Tong, L. Zhang, T. Guo, X. Liu, X. Qiao, *Appl. Opt.* **2018**, *57*, 356.
- [152] H. Liu, Y. Miao, B. Liu, W. Lin, H. Zhang, B. Song, M. Huang, L. Lin, *IEEE Sens. J.* **2015**, *15*, 3424.
- [153] S. Liu, Y. Ji, J. Yang, W. Sun, H. Li, *Sens. Actuators, A* **2018**, *269*, 313.
- [154] Y. Luo, C. Chen, K. Xia, S. Peng, H. Guan, J. Tang, H. Lu, J. Yu, J. Zhang, Y. Xiao, *Opt. Express* **2016**, *24*, 8956.
- [155] Y. Huang, W. Zhu, Z. Li, G. Chen, L. Chen, J. Zhou, H. Lin, J. Guan, W. Fang, X. Liu, *Sens. Actuators, B* **2018**, *255*, 57.
- [156] M. Bedoya, G. Orellana, M. C. Moreno-Bondi, *Helv. Chim. Acta* **2001**, *84*, 2628.
- [157] Z. L. Poole, P. R. Ohodnicki, A. Yan, Y. Lin, K. P. Chen, *ACS Sens.* **2017**, *2*, 87.
- [158] J. Dai, M. Yang, X. Yu, K. Cao, J. Liao, *Sens. Actuators, B* **2012**, *174*, 253.
- [159] Y. H. Kim, M. J. Kim, B. S. Rho, M.-S. Park, J.-H. Jang, B. H. Lee, *IEEE Sens. J.* **2010**, *11*, 1423.
- [160] S. Korposh, R. Selyanchyn, W. Yasukochi, S.-W. Lee, S. W. James, R. P. Tatam, *Mater. Chem. Phys.* **2012**, *133*, 784.
- [161] T. Wang, S. Korposh, S. James, R. Tatam, S.-W. Lee, *Sens. Actuators, B* **2013**, *185*, 117.
- [162] L. Sun, Y. Semenova, Q. Wu, D. Liu, J. Yuan, T. Ma, X. Sang, B. Yan, K. Wang, C. Yu, *J. Lightwave Technol.* **2017**, *35*, 2864.
- [163] M. Wang, M. Yang, J. Cheng, G. Zhang, C. Liao, D. Wang, *IEEE Photonics Technol. Lett.* **2013**, *25*, 713.
- [164] C. Yu, L. Liu, X. Chen, Q. Liu, Y. Gong, *Photonic Sens.* **2015**, *5*, 12.
- [165] X. Ning, J. Yang, C. L. Zhao, C. C. Chan, *Appl. Opt.* **2016**, *55*, 3543.
- [166] W. Ma, R. Wang, Q. Rong, Z. Shao, W. Zhang, T. Guo, J. Wang, X. Qiao, *IEEE Photonics J.* **2017**, *9*, 1.
- [167] J. Wu, M.-J. Yin, K. Seefeldt, A. Dani, R. Guterman, J. Yuan, A. P. Zhang, H.-Y. Tam, *Sens. Actuators, B* **2018**, *259*, 833.
- [168] P. Bhatia, B. D. Gupta, *Plasmonics* **2013**, *8*, 779.
- [169] R. Tabassum, S. K. Mishra, B. D. Gupta, *Phys. Chem. Chem. Phys.* **2013**, *15*, 11868.
- [170] S. K. Mishra, S. N. Tripathi, V. Choudhary, B. D. Gupta, *Plasmonics* **2015**, *10*, 1147.
- [171] S. K. Mishra, S. Rani, B. D. Gupta, *Sens. Actuators, B* **2014**, *195*, 215.
- [172] A. Petropoulou, S. Kralj, X. Karagiorgis, I. Savva, E. Loizides, M. Panagi, T. Krasia-Christoforou, C. Riziotis, *Sci. Rep.* **2020**, *10*, 1.
- [173] F. W. Dagnaw, W. Feng, Q.-H. Song, *Sens. Actuators, B* **2020**, *318*, 127937.
- [174] P. V. N. Kishore, S. S. Madhuvarasu, S. Moru, *Opt. Eng.* **2018**, *57*, 017101.
- [175] T.-W. Sung, Y.-L. Lo, I.-L. Chang, *Sens. Actuators, B* **2014**, *202*, 1349.
- [176] W. B. Ji, S. H. K. Yap, N. Panwar, L. L. Zhang, B. Lin, K. T. Yong, S. C. Tjin, W. J. Ng, M. B. A. Majid, *Sens. Actuators, B* **2016**, *237*, 142.
- [177] W.-B. Huang, W. Gu, H.-X. Huang, J.-B. Wang, W.-X. Shen, Y.-Y. Lv, J. Shen, *Dyes Pigm.* **2017**, *143*, 427.



**Mohamed Elsherif** holds a B.Sc. and M.Sc. in physics. He completed his Ph.D. degree in optical biosensor at the University of Birmingham, UK, in 2019. Elsherif's research interest revolves around wearable and implantable sensors for biomedical applications.



**Ahmed E. Salih** received his B.Sc. in mechanical engineering (High Honors) from the American University in Sharjah in 2018 and M.Sc. in mechanical engineering (Highest Honors) from Khalifa University in 2020. Ahmed's main area of interest is the development of hydrogel biosensors and smart contact lenses. He recently developed nanocomposite hydrogel contact lenses for color blindness management and sensing applications.



**Monserrat Gutiérrez Muñoz** holds a double Ph.D. degree: one in Materials Science from Ecole Central de Lyon, France and the second in Electrochemistry from the Research Center and Technological Development in Electrochemistry (CIDETEQ), Queretaro, Mexico. Monserrat worked as a graduate research associate at CIDETEQ and she was appointed as a postdoctoral Fellow in the Institute National des Sciences Appliquées (INSA), France. Then, she joined Honeywell Research Center, USA, as an innovation and development researcher. Currently, she is leading the nanomaterials group at Technology Innovation Institute, Abu Dhabi, UAE.



**Haider Butt** did his M.Phil. in Electrical Engineering from the University of Cambridge in 2008, followed by a Ph.D. in Nanophotonics in 2012. He was appointed as a lecturer of Nanotechnology at the Department of Mechanical Engineering, University of Birmingham, UK. He was promoted as senior lecturer in 2016 and was appointed as the senior admissions tutor for mechanical engineering in 2017. In 2019, he joined Khalifa University, UAE, as an associate professor. He has earned international recognition for his research in the area of optical sensors and carbon nanotube-based holograms.